JCI insight

# A human STAT3 gain-of-function variant confers T cell dysregulation without predominant Treg dysfunction in mice

Erica G. Schmitt, Kelsey A. Toth, Samuel I. Risma, Ana Kolicheski, Nermina Saucier, Rafael J. Feliciano Berríos, Zev J. Greenberg, Jennifer W. Leiding, Jack J. Bleesing, Akaluck Thatayatikom, Laura G. Schuettpelz, John R. Edwards, Tiphanie P. Vogel, Megan A. Cooper

*JCI Insight.* 2022. https://doi.org/10.1172/jci.insight.162695.

**Research** In-Press Preview **Immunology**

Primary immune regulatory disorders (PIRD) are a group of disorders characterized by immune dysregulation, presenting with a wide range of clinical disease including autoimmunity, autoinflammation, or lymphoproliferation. Autosomal dominant germline gain-of-function (GOF) variants in *STAT3* result in a PIRD with a broad clinical spectrum. Studies in patients have documented a decreased frequency of FOXP3$^+$ regulatory T (Treg) cells and an increased frequency of Th17 cells in some patients with active disease. However, the mechanisms of disease pathogenesis in STAT3 GOF syndrome remain largely unknown, and treatment is challenging. We developed a knock-in mouse model harboring a de novo pathogenic human STAT3 variant (p.G421R) and found these mice developed T cell dysregulation, lymphoproliferation and CD4$^+$ Th1 cell skewing. Surprisingly, Treg cell numbers, phenotype, and function remained largely intact, however mice had a selective deficiency in the generation of iTreg cells. In parallel, we performed single-cell RNA-sequencing on T cells from STAT3 GOF patients. We demonstrate only minor changes in the Treg cell transcriptional signature and an expanded, effector CD8$^+$ T cell population. Together, these findings suggest Treg cells are not the primary driver of disease and highlight the importance of preclinical models in the study of disease mechanisms in rare PIRD.



# A human STAT3 gain-of-function variant confers T cell dysregulation without predominant Treg dysfunction in mice

Erica G. Schmitt[1], Kelsey A. Toth[1], Samuel I. Risma[1], Ana Kolicheski[1], Nermina Saucier[1], Rafael J. Feliciano Berríos[2], Zev J. Greenberg[3], Jennifer W. Leiding[4], Jack J. Bleesing[5], Akaluck Thatayatikom[6], Laura G. Schuettpelz[3], John R. Edwards[2], Tiphanie P. Vogel[7], and Megan A. Cooper[1,8]

[1]Department of Pediatrics, Division of Rheumatology and Immunology, Washington University School of Medicine, St. Louis, MO, USA.
[2]Center for Pharmacogenomics, Department of Medicine, Washington University School of Medicine, St. Louis, MO, USA.
[3]Department of Pediatrics, Division of Hematology and Oncology, Washington University School of Medicine, St. Louis, MO, USA.
[4]Division of Allergy and Immunology, Department of Pediatrics, Johns Hopkins University, Baltimore, MD and Infectious Diseases and Immunology, Arnold Palmer Hospital for Children, Orlando, FL, USA.
[5]Division of Bone Marrow Transplantation and Immune Deficiency, Cincinnati Children's Hospital Medical Center, Cincinnati, OH; Department of Pediatrics, University of Cincinnati College of Medicine, Cincinnati, OH, USA.
[6]AdventHealth for Children, Orlando, FL, USA.
[7]Division of Rheumatology, Department of Pediatrics, Baylor College of Medicine and Texas Children's Hospital, Houston, TX, USA.
[8]Department of Pathology and Immunology, Washington University School of Medicine, St. Louis, MO, USA.

Corresponding author: Megan A. Cooper, 660 S. Euclid Ave, Box 8208, Washington University School of Medicine, St. Louis, MO 63110; e-mail: cooper_m@wustl.edu. Phone: 314-454-6124 Fax: 314-286-2895

The authors have declared that no conflict of interest exists.

**Abstract**

Primary immune regulatory disorders (PIRD) are a group of disorders characterized by immune dysregulation, presenting with a wide range of clinical disease including autoimmunity, autoinflammation, or lymphoproliferation. Autosomal dominant germline gain-of-function (GOF) variants in *STAT3* result in a PIRD with a broad clinical spectrum. Studies in patients have documented a decreased frequency of $FOXP3^+$ regulatory T (Treg) cells and an increased frequency of Th17 cells in some patients with active disease. However, the mechanisms of disease pathogenesis in STAT3 GOF syndrome remain largely unknown, and treatment is challenging. We developed a knock-in mouse model harboring a *de novo* pathogenic human STAT3 variant (p.G421R) and found these mice developed T cell dysregulation, lymphoproliferation and $CD4^+$ Th1 cell skewing. Surprisingly, Treg cell numbers, phenotype, and function remained largely intact, however mice had a selective deficiency in the generation of iTreg cells. In parallel, we performed single-cell RNA-sequencing on T cells from STAT3 GOF patients. We demonstrate only minor changes in the Treg cell transcriptional signature and an expanded, effector $CD8^+$ T cell population. Together, these findings suggest Treg cells are not the primary driver of disease and highlight the importance of preclinical models in the study of disease mechanisms in rare PIRD.

## Introduction

Immune dysregulation arises when there is a disruption of immunological tolerance or alterations in the mechanisms utilized to downregulate the immune response after an insult. Discovery of monogenic inborn errors of immunity (IEI) presenting predominantly with immune dysregulation rather than susceptibility to infection, have led to important findings about key factors regulating the human immune response. These disorders, known as primary immune regulatory disorders (PIRD), present with a wide range of clinical disease for example, early-onset autoimmune disease, hemophagocytic lymphohistiocytosis (HLH), autoinflammatory syndromes, very early-onset inflammatory bowel disease, and/or lymphoproliferation (1-3). Loss of T cell tolerance is a mechanism for several PIRD. For instance, disruption of regulatory T (Treg) cells due to deleterious variants in the *FOXP3* gene result in immune dysregulation, polyendocrinopathy, enteropathy, X-linked (IPEX) syndrome, which is characterized by multi-organ autoimmunity due to loss of peripheral tolerance from absent or dysfunctional Tregs (4-8). IPEX syndrome was the first PIRD characterized in a group of monogenic disorders resulting in Treg defects, sometimes termed "Tregopathies" (9). Discovery and investigation of pathogenic human *FOXP3* variants has provided key insights into structural protein domains and the function of FOXP3. As another example, patients with autoimmune polyendocrinopathy with candidiasis and ectodermal dystrophy (APECED) were found to have defects in the gene *AIRE*, encoding an important transcription factor, a discovery which ultimately led to new insights into thymic expression of tissue-specific transcripts and central tolerance (10-12). Interestingly, while there is clinical overlap between IPEX and APECED, for example endocrinopathies, the means by which T cell tolerance is altered are quite distinct, demonstrating how monogenic disease with clinical overlap can have different immunologic mechanisms. Thus, studying PIRD

93 is not only instrumental for elucidating disease pathogenesis and treatment strategies for
94 individual patients, but also can provide context for understanding key immunological
95 mechanisms.
96
97 Autosomal dominant germline gain-of-function (GOF) variants in STAT3 result in a PIRD
98 characterized by immune dysregulation and a broad spectrum of clinical features including
99 cytopenias, lymphadenopathy, interstitial lung disease, enteropathy, and polyendocrinopathy (13,
100 14). STAT3 is a highly conserved transcription factor downstream of multiple cytokines and
101 growth factors and signaling through activated, phosphorylated STAT3 homodimers is
102 implicated in both pro- and anti-inflammatory pathways (15). STAT3 is also a key transcription
103 factor involved in the regulation and balance of the Treg/ T helper (Th) 17 cell polarization axis
104 (16). A decreased frequency of $FOXP3^+$ Treg cells has been observed in the peripheral blood of
105 some, but not all, STAT3 GOF patients and, taken together with the overlapping clinical features
106 in STAT3 GOF and IPEX syndrome, it has been suggested that this disease falls within the
107 spectrum of Tregopathies (9, 13). However, whether decreased numbers of Treg cells in the
108 peripheral blood are a primary cause of disease and if there are intrinsic defects in Treg
109 generation, as in IPEX syndrome, is unknown. Confirming Treg cell defects as a primary cause
110 of disease pathogenesis would have an impact on the approach to treatment in patients with
111 STAT3 GOF syndrome, for instance, cell-based therapies such as autologous gene therapy, or
112 Treg cell-based therapies.
113
114 To further investigate the role of STAT3 GOF in immune dysregulation and Treg cells, we
115 developed a mouse model of STAT3 GOF with a DNA-binding domain variant identified in

patients, p.G421R, on the C57BL/6J background. Patients with this variant have presented with multiorgan involvement, including autoimmune cytopenias, lymphadenopathy, hepatosplenomegaly, autoimmune hepatitis, scleroderma, polyarthritis, respiratory infections, enteropathy and short stature (13, 17-19). Using this mouse model, we performed a series of phenotypic and functional studies, focusing on Treg cells, given the previously noted Treg cell deficiency in patients. We found that the variant imparts progressive lymphoproliferation in affected mice, with an expansion of CD4 and CD8 T effector memory cells. Interestingly, STAT3 GOF mice had normal to increased Treg cell numbers, but the ability to generate induced Treg (iTreg) cells was selectively impaired. STAT3 GOF Treg cells were otherwise similar to WT, with only minor differences seen in disease models and transcriptional signatures. Surprisingly, further analysis of CD4 subsets in a colitis disease model and bone marrow chimera demonstrated a Th1-skewed effector CD4 T cell compartment, but no increase in Th17 cells. Finally, we examined the transcriptional signature of humans with STAT3 GOF syndrome using single cell RNA-sequencing. Collectively, these data have implications for disease paradigms and treatment targets going forward, specifically, Treg centered therapies may be insufficient in STAT3 GOF syndrome, and the surprising finding of a Th1 signature in this disease model.

## Results

*Heterozygous G421R mice recapitulate aspects of human disease*

To investigate the pathogenesis of STAT3 GOF syndrome we developed a mouse model of the disease-causing p.G421R DNA-binding domain variant. Mice were generated using CRISPR/CAS9 technology to introduce a single nucleotide change (Figure 1A). The point mutation, c.1261G>A, was verified by Sanger sequencing (Figure 1B), and mice were fully back-crossed to the C57BL/6 background. Male and female mice heterozygous for the p.G421R variant (*Stat3*$^{p.G421R/+}$, subsequently referred to as STAT3 GOF or G421R mice) had a similar weaning weight compared to WT counterparts, and survival and breeding were not impaired (Figure 1C). Interestingly, mice homozygous for the p.G421R variant were runted, and died shortly after the time of weaning (Figure 1C). To determine the impact of the p.G421R variant on STAT3 activity in heterozygous mice, STAT3 phosphorylation was measured in naïve splenic $CD4^+$ and $CD8^+$ T cells. At baseline or with IL-6 stimulation, p-STAT3 was similar in splenic T cells from STAT3 GOF mice and littermate controls (Figure 1D). However, consistent with findings in a patient with the p.G421R variant, there was delayed dephosphorylation of STAT3 in T cells from STAT3 GOF mice (Figure 1D) (13). Collectively, these data demonstrate that the p.G421R variant results in STAT3 GOF in mice.

The immune phenotype of the mice was analyzed at different stages of development, including young (<6wk of age), adult (age 7-16wk), and old (>20wk) mice. Young mice had normal counts and populations of CD4 and CD8 T cells develop in the thymus (Figure 1E, S1A). Thymic CD4 and CD8 T cell frequencies and CD4 SP and CD8 SP T cell maturation were similar, on a global

level, in WT and STAT3 GOF mice (Figure S1B). Unexpectedly, mice homozygous for the STAT3 p.G421R variant had a significantly reduced thymus size (Figure S1C).

Young mice (<6 wk of age) had a normal spleen size (Figure S1D), however by adulthood (age 7-16 wk), significant splenomegaly was observed (Figure 1F). A similar frequency of CD4, CD8 and CD19 lymphocytes were observed in the spleens of WT and STAT3 GOF mice, but there were increased numbers of these cell subsets (Figure 1F, data not shown). Aged mice (>20 weeks) demonstrated a similar pattern of splenomegaly and increased numbers of T and B lymphocytes (data not shown). STAT3 GOF mice also developed lymphadenopathy as they reached maturity (Figure 1G), with a reduction in the CD8 T cell frequency but overall increased numbers of CD4, CD8 and CD19 lymphocytes (data not shown). In the lymph nodes of aged mice, there was a relative decrease in the frequency of T cells (CD4, CD8) and an increase in the frequency of $CD19^+$ B cells, however, cell counts for all of these populations were increased in the STAT3 GOF mice (Figure S1E, data not shown).

While young STAT3 GOF mice did not have lymphoproliferation, there was evidence of immune dysregulation at this early timepoint, with an increased frequency of $CD44^+CD62L^-$ activated, effector CD4 and CD8 T cells (Figure 2A). These cells continued to accumulate and increased with aging (Figure 2B,C). STAT3 GOF mice had a significant increase in $CD3^+CD4^+CD44^+$ cells that were Ki-$67^+$, suggesting increased proliferation of this population (Figure S1F). Splenic T cells from mice homozygous for the STAT3 GOF variant also displayed an activated, effector phenotype at a young age (Figure 2A). Overall, these data suggest that

183 STAT3 GOF mice recapitulate many aspects of STAT3 GOF syndrome, including
184 lymphoproliferation with splenomegaly and lymphadenopathy.
185
186 $CD4^+$ T cells isolated from patients with STAT3 GOF syndrome have been shown to produce
187 pro-inflammatory cytokines, such as IL-17, and this pathway has garnered particular interest
188 given the role of STAT3 in Th17 cell development (13). In at least one instance, however, $CD4^+$
189 T cells from patients with STAT3 GOF syndrome have also been shown to produce IFN-γ with
190 stimulation (20). Therefore, we examined cytokine production in STAT3 GOF mice in response
191 to ex vivo stimulation with PMA/Ionomycin. Unexpectedly, there was an increased frequency of
192 IFN-γ-producing cells among splenic $CD4^+$ T cells isolated from mice homozygous for the
193 STAT3 GOF variant (Figure 2D). In vitro differentiation of naïve T cells under Th1-polarizing
194 conditions revealed a mild reduction in the ability of STAT3 GOF T cells to differentiate into
195 IFN-γ-producing cells (Figure S1G). In ex vivo stimulated cells, $CD4^+$ T cell Th1 polarization
196 was seen in adult mice heterozygous for the variant, and was further exaggerated in aged mice
197 (Figure 2E). There were no differences in ex vivo IL-17A-producing cells. These data reveal a
198 dysregulated, Th1 response in STAT3 GOF mice.
199
200 To study whether the observed T cell phenotype was cell intrinsic, bone marrow chimeras were
201 generated. Congenic $Ly5.1^+$ lethally irradiated hosts were reconstituted with bone marrow from
202 WT or homozygous STAT3 GOF mice ($Ly5.2^+$). Mice were analyzed 12 weeks after
203 reconstitution. Mice transplanted with homozygous bone marrow survived to the conclusion of
204 the experiment and had good engraftment of donor bone marrow in the peripheral blood by 10
205 weeks post-transplant (Figure S1H). Similar to mice receiving WT bone marrow, splenocytes

isolated from mice transplanted with bone marrow from homozygous mice were comprised largely of donor Ly5.2$^{+}$ cells (Figure 2F). Strikingly, the dysregulated T cell phenotype was preserved. Mice that received homozygous STAT3 GOF bone marrow had an increased frequency of CD44$^{+}$CD62L$^{-}$ activated, effector CD4 and CD8 T cells in the spleen (Figure 2G). There was also an increased frequency of IFN-γ-producing cells among splenic CD4$^{+}$ T cells derived from STAT3 GOF homozygous donors (Figure 2H). This suggests that T cell intrinsic defects contribute to the observed phenotype in STAT3 GOF mice.

*STAT3 GOF Treg cells are not substantially altered*

Prior studies in humans with STAT3 GOF syndrome suggest that these patients may have defects in FOXP3$^{+}$ Treg cells; this is based on studies demonstrating reduced Treg cell frequency in the peripheral blood of patients, organ-specific autoimmunity (i.e. enteropathy, type 1 diabetes, cytopenias), and in some instances, reduced Treg cell suppressive capacity in vitro (9, 13, 14, 20, 21). To characterize Treg cells in STAT3 GOF mice, mice were crossed to *Foxp3*$^{EGFP}$ reporter mice, which accurately identifies Foxp3$^{+}$ Treg cells with EGFP (22). The frequency and number of Treg cells was similar in the thymus of WT and STAT3 GOF mice (Figure S2A). Interestingly, an increased frequency of Treg cells was seen in the thymus of STAT3 GOF homozygous mice, though given the reduction in the size of the thymus, Treg cell numbers were significantly reduced (Figure S2A). Treg cell frequency and number were similar in the spleen of young mice (Figure S2B). In adult mice, Treg cell frequency and numbers were normal, and in some cases increased, in the tissues examined, spleen, peripheral lymph node (LN), mesenteric lymph node (MLN), and blood (Figure 3A). With aging, there was a progressive increase in the frequency and number of Treg cells in the peripheral lymph nodes (Figure 3B).

Aged STAT3 GOF mice also accumulated an increased number of Treg cells in the spleen (Figure S2C). In contrast to STAT3 GOF patients with active disease, peripheral blood $Foxp3^{+}CD25^{+}$ Treg cell frequencies were normal in this model (Figure 3C).

The phenotype of the STAT3 GOF Treg cells was assayed by flow cytometric analysis of several canonical Treg cell markers. The frequency of Treg cells in the LN expressing each marker, as well as the median fluorescence intensity of CD25, CD44, CD62L, CTLA-4, Helios, and CD103 were similar between WT and STAT3 GOF Treg cells (Figure 3D). However, there was a small but significantly increased frequency of $GITR^{+}$ Treg cells in the LN of STAT3 GOF mice, and the MFI of GITR was also increased on these Treg cells (Figure S2D). There was also an increased frequency of $CD103^{+}$ Treg cells in the spleen of STAT3 GOF mice, and the MFI level of CD103 was similarly elevated (Figure S2E). The function of ex vivo isolated STAT3 GOF Treg cells was assessed using an in vitro suppression assay, with suppressive capability measured by the ability of Treg cells to inhibit cell division induced by TCR stimulation. Here, STAT3 GOF Treg cells performed similar to WT Treg cells (Figure 3E).

We then tested the ability of STAT3 GOF T cells to upregulate Foxp3 in vitro, and generate iTreg cells upon stimulation with anti-CD3, anti-CD28, TGF-β and IL-2. Interestingly, STAT3 GOF T cells had a significantly reduced capacity to generate iTreg cells in vitro (Figure 3F). In vitro conversion was titratable with increasing doses of anti-CD3 in both WT and STAT3 GOF mice (Figure S2F). At low concentrations of anti-CD3, where iTreg conversion was not optimized, WT and STAT3 GOF T cells had similar upregulation of Foxp3 (Figure S2F). Overall, these mice, maintained in a specific pathogen-free facility developed

lymphoproliferation, but Treg cell enumeration, phenotype, and function was only minimally impacted and they did not develop other clinical disease manifestations. A selective defect in iTreg cell generation was uncovered, and this reduced capacity to generate iTreg cells may be relevant for immune dysregulation under conditions that stress the system. Therefore, we next evaluated the Treg cell epigenetic and transcriptional signatures, and in vivo function.

*STAT3 GOF and WT Treg cells have a similar epigenetic and transcriptional profile*

Epigenetic regulation of the *Foxp3* locus is important for establishment of Treg cell stability and identity (23, 24). Hypomethylation of the Treg-specific demethylation region (TSDR), located ~4kb downstream of the *Foxp3* promoter in the conserved noncoding sequence 2 (CNS2) of the *Foxp3* locus, is critical for stable and heritable Foxp3 expression (25). The impact of STAT3 GOF on TSDR methylation was measured by bisulfite sequencing using WT naïve T cells, WT Treg, and STAT3 GOF Treg cells isolated from the spleen and peripheral lymph nodes of male mice. Cells from male mice were used due to random X-inactivation of the *Foxp3* gene in female mice.

A region of the CNS2 within the TSDR was amplified and sequenced by next-generation sequencing. Conversion of non-methylated cytosine residues to uracil was achieved at an efficiency of >99%. At any given CpG, the sequencing coverage ranged from 16,857 to 49,178 reads. As expected, WT naive T cells were highly methylated at the 10 CpG sites examined (ranging from 95-97% methylation). WT Treg cells had low levels of methylation at the 10 CpG sites (methylation 9-13%), and this pattern was not different from Treg cells isolated from STAT3 GOF mice (methylation 5-10%) (Figure 4A, top). Methylation signatures from

individual mice overall, were very similar (Figure 4A, bottom). Additional analysis of sorted Treg cells from the thymus of WT and STAT3 GOF mice demonstrated similar levels of methylation in these populations (Figure S3A). At any given CpG, the sequencing coverage ranged from 32,318 to 69,152 reads. In the thymus, WT Treg cells had intermediate levels of methylation at 10 CpG sites (methylation 39-67%), and this was similar to STAT3 GOF Treg cells (methylation 34-67%). This degree of methylation is in line with what is reported in the literature for bulk thymic Treg cells, and implies that STAT3 GOF Treg cells are able to undergo progressive demethylation with maturation (26).

Studies suggest that the Treg-specific transcriptional program is regulated not only by Foxp3 binding, but that Foxp3 likely acts in conjunction with other cofactors, such as GATA3 and STAT3 (27-29). Wild-type STAT3, in its activated phosphorylated state, has been shown to interact with Foxp3. Treg-specific expression of STAT3 is critical for control of pathogenic Th17 responses and alterations in the Treg transcriptional program, including alterations in key chemokine receptors and suppressor molecules, may underlie this observation (30). To further investigate the impact of STAT3 GOF on Treg cells, RNA-sequencing was performed on sorted $Foxp3^+$ Treg cells from the spleen and lymph nodes of WT and STAT3 GOF mice. Interestingly, *Igfbp4* was the only transcript with a significant difference based on adjusted p-value, with a 1.2 log2 fold change between WT and STAT3 GOF Treg cells for this transcript (Figure 4B). We specifically examined the differential expression of a set of 320 canonical Treg cell signature genes, and found no significant differences (log2 fold change $>1.5$ or $< -1.5$, adjusted $p<0.05$) between WT and STAT3 GOF Treg cells (Figure 4C) (27). Overall, under homeostatic

297 conditions, there were not major differences observed in the transcriptome of STAT3 GOF Treg
298 cells.
299
300 *STAT3 GOF T cells adopt a Th1 phenotype and iTreg cells are reduced in a disease model*
301 A T cell transfer model of colitis was utilized to test T cell function in a disease setting. Naïve
302 $CD4^+$ T cells ($4x10^5$ $CD4^+$ $EGFP^-CD45RB^{hi}$ cells) were isolated by cell sorting from WT or
303 STAT3 GOF mice and adoptively transferred into C57BL/6 *Rag1*$^{-/-}$ mice (Figure 5A). Weight
304 loss and survival were similar between mice that received WT or STAT3 GOF T cells (Figure
305 5B, C, S4A). Mice that received either cell type had a significant reduction in weight by day 28
306 after transfer, as compared to control C57BL/6 *Rag1*$^{-/-}$ mice (Figure 5B). Therefore, initial
307 analysis was focused on this early time point. Phenotypic analysis of transferred T cells after 28
308 days demonstrated an increased frequency of IFN-$\gamma^+$ cells, but not IL-17A-producing cells, in the
309 intestine lamina propria and mesenteric lymph nodes of mice receiving STAT3 GOF T cells
310 (Figure 5D, E). Spleen, MLN and intestinal lamina propria cell counts were similar at this early
311 time point (Figure S4B). Notably, after 28 days, mice with colitis induced by STAT3 GOF T
312 cells had a significant reduction in the frequency of peripherally-induced Treg (pTreg) cells in
313 the mesenteric lymph nodes and intestinal lamina propria, suggesting decreased formation of
314 pTreg cells in vivo, which was consistent with the in vitro data (Figure 5F). Strikingly, mice that
315 received STAT3 GOF T cells and survived to the conclusion of the experiment (70d), had an
316 ~11-fold reduction in formation of in vivo-derived pTreg cells in the spleen and ~6-fold
317 reduction of pTreg cells in the MLN (Figure 5G,H). Total cell counts in the spleen were similar,
318 but mice that received STAT3 GOF naïve T cells had a decreased MLN total cell count (Figure
319 S4C). These results imply the surprising finding that STAT3 GOF T cells skew toward a Th1

phenotype, both in this disease model and in mice with germline STAT3 GOF. In addition, these data support the in vitro data, again demonstrating an impairment in pTreg cell induction.

*STAT3 GOF Treg cells are functional in vivo*

To establish the impact of STAT3 GOF on Treg cell function in vivo, we again utilized the T cell transfer model of colitis, as the role of Treg cells in treating and preventing disease in this model has been well-established (31, 32). There are some limitations of this model on the C57BL/6J background due to impaired pTreg cell and Th17 cell generation, however murine genetic models are often created on the C57BL/6J background and this colitis model remains useful for assessing Treg cell function in vivo (33). As demonstrated in the prior studies, by experimental day 28, colitis mice had significant weight loss compared to controls (Figure 5B). Therefore, mice with colitis induced by the transfer of $4x10^5$ WT $CD4^+Ly5.1^+EGFP^-CD45RB^{hi}$ cells were treated with either WT or STAT3 GOF Treg cells on day 21. Mice were treated with $1x10^6$ Treg cells that were isolated from either WT or STAT3 GOF mice ($Ly5.2^+$) harboring the *Foxp3*$^{EGFP}$ reporter to allow for sorting of a purified Treg cell population (Figure 6A). Weight change of individual mice within each experimental group was variable (Supplemental Figure S5A), however pairwise comparison at the indicated timepoints demonstrated that mice treated with WT Treg cells had improved weight gain compared to untreated mice, beginning at day 77 ($p=0.0473$). Mice treated with STAT3 GOF Treg cells had a trend toward improved weight gain by day 42, but the group comparisons did not reach significance ($p=0.0583$) (Figure 6B). However, mice treated with STAT3 GOF Treg cells actually had improved survival (Figure 6C). Spleen and MLN cell counts did not differ significantly between untreated and treated mice (Figure S5B). The recovery of Ly5.1 and Ly5.2 marked cell populations was similar in the

spleens of treated mice (Figure 6D). Conversely, in the MLN there was an increased frequency of Ly5.1 cells used to induce colitis and a corresponding decreased frequency of Ly5.2 cells in mice treated with STAT3 GOF Treg cells. The ratio of Ly5.1:Ly5.2 cells recovered in the MLN of treated mice was significantly higher in mice treated with STAT3 GOF Treg cells compared to those treated with WT Treg cells (14.9 vs 3.6, respectively), suggesting that local control of colitis cell accumulation may be impaired in these mice (Figure 6D).

Indeed, the frequency of Treg cells found in the spleen and MLN of mice treated with STAT3 GOF Treg cells was reduced compared to mice treated with WT Treg cells (Figure 6E, F). However, this did not correlate with an increased frequency of ex-Treg cells, defined as cells that were $Ly5.2^{+}EGFP^{-}$ (Figure S5C). Interestingly, the frequency of MLN Ly5.1 cells producing IL-17A was increased in mice treated with STAT3GOF Treg cells, as compared to untreated mice (Figure 6G). In the spleen, IL-$17A^{+}Ly5.1^{+}$ cells were increased in both groups of treated mice compared to untreated mice (Figure S5D). Although the frequency of ex-Treg cells was similar in mice treated with WT or STAT3 GOF Treg cells, a higher frequency of STAT3 GOF ex-Treg cells produced IL-17A (Figure 6H).

In summary, STAT3 GOF Treg cells improved survival in a mouse model of experimental colitis, despite impaired Treg cell recovery and control of $Ly5.1^{+}$ T cell accumulation and IL-17A secretion. Furthermore, ex-Treg cells from STAT3 GOF mice demonstrate dysregulated production of IL-17A. This suggests that in situations where the system is stressed, Treg cell function may not be normal.

*Single Cell RNA-sequencing of STAT3 GOF Patient T cells*

To explore the dysregulated T cell phenotype in human STAT3 GOF syndrome, T cells were isolated from the peripheral blood of 3 healthy age- and sex-matched donors (C1-C3) and 3 patients with STAT3 GOF syndrome (P1-P3). Cells were rested in media or stimulated with anti-CD3/CD28 (C1s-C3s, P1s-P3s) for 16 hours and then subjected to single-cell RNA-sequencing analysis. Human STAT3 variants were located throughout the protein and included variants in the DNA-binding domain p.T389S (c.1165A>T) in patient 1 (P1), the NT domain p.R70H (c.209G>A) in patient 2 (P2), and the coiled-coil domain p.F174S (c.521T>C) in patient 3 (P3). Additional details regarding the patients can be found in Supplemental Table 1. All patients were on immunosuppressive therapy, patients P1 and P2 were stable, but P3 had progressive disease, and samples were obtained at a single point in time, which are limitations for interpretation of the data.

Unsupervised dimensionality reduction analysis of single cell RNA-sequencing transcriptome data from STAT3 GOF and healthy controls identified 24 unique clusters (Figure 7A,B). After the initial filtering steps, a total of 140,931 cells were analyzed. Clusters 8, 11, 17, and 24 were enriched (at least 60% of the cells) for cells from STAT3 GOF patients (Figure 7C, S6A). Clusters 10 and 11 were dominated by cells from patient samples P3 or P3s (>50% of cells in the cluster) (Figure 7C, S6B).

Cell populations were further identified by their expression of canonical cell markers using the Azimuth human PBMC reference to predict cell types (NIH Human Biomolecular Atlas Project HuBMAP) (34). All cells predicted as T cells (total of 139,421 cells) were segregated according

389 to affected status, as well as on the presence or absence of stimulation (Figure 7D, E).
390 Regulatory T cells were identified based on expression of *RTKN2, FOXP3, AC133644.2, CD4,*
391 *IL2RA, TIGIT, CTLA4, FCRL3, LAIR2,* and *IKZF2*. Treg cells dominated clusters 18, 19, and 20
392 (Figure S6C). Differential expression analysis of all cells classified as Treg cells revealed 59
393 genes differentially expressed between control and STAT3 GOF patients in the unstimulated
394 samples and 112 genes with significant differential expression in the stimulated samples (Figure
395 7F). In the unstimulated Treg cells, genes overexpressed in STAT3 GOF patients included
396 *NDUFA12, GPR171, ITGA4, TNFRSF13B, TRAT1, LPIN2,* and *CD7* and also, primarily in
397 patient sample P3, *CCL5, IRF1, STAT1,* and *STAT3* (Figure 7F, left). In the stimulated Treg
398 cells, there was similarly increased expression of *NDUFA12, ITGA4,* and *TNFRS13B*, but also
399 increased expression of *TIGIT, IL32, FOXP3, LTB, CXCR4, IL12RB2*, in STAT3 GOF samples
400 and decreased *CD69* and *IL4R* (Figure 7F, right). Overall, small differences in the average log2
401 fold change were observed, suggesting that the circulating Treg cells in control and patient
402 samples were similar.
403
404 Among "Treg signature" genes identified in a published data set (35), 322 of 367 genes (total of
405 386 probesets) were found in our dataset. There were only significant differences in the
406 expression of 7 transcripts, including *GBP5, RTKN2, CCL5, TRAT1, GBP2, TSHZ2*, and
407 *ARID5B*. Expression differences noted for *CCL5* and *GBP5* were primarily due to changes seen
408 in sample P3, and alterations in *TSHZ2* expression were due to sample P2 (Figure 7G, left).
409 Expression of the "Treg Signature" was analyzed within the stimulated Treg cell subset, with 11
410 differentially expressed transcripts, including *TIGIT, FOXP3, LRRN3, IL12RB2, RTKN2, ANK3,*
411 *IL4R, SAT1, BIRC3, GBP5,* and *LGALS3* (Figure 7G, right).

We further examined the CD4 T central memory (TCM) subset (defined by expression of *IL7R, TMSB10, CD4, ITGB1, LTB, TRAC, AQP3, LDHB, IL32, MAL*) because this was heavily represented in multiple clusters. 45 unique transcripts were differentially expressed between unstimulated control and STAT3 GOF CD4 TCM cells genes (adjusted $p<0.05$, average log2 fold change >0.25 or < –0.25). Transcripts identified as overexpressed in STAT3 GOF again included *TNFSF13B* and *ITGA4* as well as *ARID5B, LIMS1, TNFAIP3* and in sample P3, *STAT1* and *IRF1* (Figure 8A). Examination of enriched ontology clusters found significant enrichment in several pathways, with cellular response to cytokine stimulus, aerobic glycolysis, and interferon gamma signaling amongst those pathways with the most significant p-values (Figure S6D).

In stimulated CD4 TCM cells, there were 57 differentially expressed transcripts (adjusted $p<0.05$, average log2 fold change >0.25 or < –0.25). Transcripts identified as overexpressed in STAT3 GOF included *TIGIT, CXCR4, ITGA4, KLF6,* and *IL7R*. Transcripts underexpressed in STAT3 GOF patients compared to controls included *IL2, TNF, LTA, CD69, IRF8,* and *BCL2A1* (Figure 8A, right). Enriched ontology clusters analysis performed with genes overexpressed in STAT3 GOF stimulated TCM cells demonstrated enriched terms for antigen processing and presentation of endogenous peptide antigen via MHC I, negative regulation of immune system process, and regulation of cell-cell adhesion, amongst others (Figure S6E).

Clusters that were dominated by cells from samples P3/P3s were largely identified as CD8 T cells, including CD8 TCM and CD8 T effector memory (TEM), as well as γδ T cells. For

example, cluster 10, a cluster made up of stimulated cells, largely consists of cells from sample P3s. These cells are identified as CD8 TEM and γδ T cells by the azimuth program. Cluster 11 is largely dominated by unstimulated cells, particularly from patient sample P3 (~73% of cells). This cluster identifies primarily as CD8 TEM cells (~95% of cells). The CD8 TEM cells were identified based on expression of transcripts for *CCL5, GZMH, CD8A, TRAC, KLRD1, NKG7, GZMK, CST7, CD8B,* and *TRGC2*. Here, differential expression analysis revealed increased expression of 245 genes and decreased expression of 97 genes in STAT3 GOF compared to controls (Figure 8B). Those genes noted to have increased expression included *GNLY, GZMH, PRF1, GZMB, KLRD1, CX3CR1,* and *STAT3*. Gene list analysis of those genes upregulated in cluster 11 STAT3 GOF cells identified enriched ontology clusters including cytokine signaling in immune system and cell activation, but also positive regulation of the immune response and cytokine production, as well as the IL-12 pathway (Figure S6F). Accordingly, there was also a relative decrease in clusters that were identified as naïve T cells, including cluster 0 (mostly naïve CD4 T cells), cluster 1 (stimulated CD4 naïve and TCM cells), and clusters 3 and 6 (naïve CD8 T cells).

In summary, the expression of canonical Treg cell genes in healthy control Tregs and Tregs from treated patients with STAT3 GOF syndrome were similar, with only small differences in average log2 fold change observed in a few select genes. These data support the patterns seen in the murine data, and suggest that STAT3 GOF confers a mild impact on circulating Treg cells and on the composition and transcriptomic profile of circulating T cells.

## Discussion

In this study, we generated a mouse model of a human STAT3 GOF variant to study the impact of STAT3 GOF on T cells, with a focus on Treg cells. We demonstrate that CD4 and CD8 T cell dysregulation commences early in development, culminating in lymphoproliferative disease and Th1-dominated $CD4^+$ T cell skewing. However, Treg cell numbers, function, and phenotype were only mildly impacted. Specifically, we observed an accumulation of Treg cells paralleling the lymphoproliferation, and a defect in the generation of iTreg cells. Lastly, we studied the immune phenotype of patients with STAT3 GOF syndrome, also demonstrating a mild Treg cell impact by single-cell RNA-sequencing, as well as an expanded $CD8^+$ T effector memory population.

Although a reduction in Treg cell numbers and/or function has been implicated as an etiology of autoimmunity, increased numbers of Treg cells have also been observed in several autoimmune diseases, suggesting that, in some instances, Treg cell expansion and/or induction may actually attempt to constrain disease progression (36, 37). Indeed, in other models of organ-specific autoimmunity, partial Treg cell depletion promotes disease progression and death, supporting the importance of Treg cell presence at sites of inflammation (38). Data on human Treg cells in disease is largely limited to peripheral blood specimens, as studying local Treg cell generation and enumeration in patients is often not feasible. The impact of chronic inflammation on Treg phenotype, function, and deviation from an anti-inflammatory role remains under investigation (39). A Treg cell defect has been implicated in the pathogenesis of STAT3 GOF syndrome based on the clinical phenotype of patients with active disease, and with peripheral blood specimens demonstrating reduced Treg numbers or reduced CD25 expression, and in a handful of patients,

481 reduced Treg function (9, 14). Our data do not support the hypothesis that inherent defects in
482 Tregs are the main driver of disease, but rather, align with a recently published murine model of
483 a diabetogenic STAT3 GOF variant (40). In this study, a knock-in mouse model on the nonobese
484 diabetic background was created using a STAT3 GOF DNA-binding domain variant (p.K392R)
485 (40). While Treg cell generation was impaired in vitro, functional analysis of Treg cells in an
486 antigen-specific system did not implicate Treg cells as key drivers of disease. Rather, this group
487 identified a clonally expanded, pathogenic CD8 effector T cell population and CD8 T cell
488 dysregulation as a key component of type 1 diabetes development. We also identified an
489 increased frequency of activated, effector CD8 T cells in murine secondary lymphoid organs.
490 Furthermore, our single-cell RNA-sequencing data from STAT3 GOF patients demonstrated an
491 expanded cluster in one patient that was comprised primarily of CD8 TEM cells with increased
492 expression of several CD8 cytotoxic, effector transcripts compared to control samples.
493 Accordingly, preclinical models examining underlying disease mechanisms are essential to
494 understanding disease pathogenesis and treatment strategies in rare diseases such as IEI.
495
496 Precision medicine for IEI, for example with small molecules or biologics, presents a challenge
497 as the rarity of these disorders make it difficult to perform controlled trials. Therefore, in depth
498 knowledge of underlying immunological mechanisms of disease is needed to help guide clinical
499 decision making and inform on the utility of repurposing currently available medications for
500 IEIs. STAT3 is a highly conserved protein, with only one amino acid different between mouse
501 and human (a tolerated substitution of aspartic acid for glutamic acid at the C terminus,
502 Uniprot.org), suggesting that the mouse is a good model organism to study STAT3-mediated
503 disease. Indeed, a mouse model of *STAT3* loss-of-function (hyper IgE syndrome) recapitulated

many aspects of disease including impaired Th17 cells, and mouse models of IPEX and APECED have proved useful as tools for studying T cell tolerance (12, 41, 42). Autosomal dominant PIRDs, like STAT3 GOF, demonstrate profound clinical heterogeneity and likely there are additional factors contributing to disease (such as genetic or environmental) that are not readily apparent in a controlled, inbred animal model.

There is ongoing interest and clinical efforts to harness the therapeutic potential of Treg cells for the treatment of autoimmunity and IEI (43-45). Particularly in rare IEI with immune dysregulation, it is critical to understand whether a defect in Treg cell generation or function exists, prior to proceeding with Treg cell-targeted therapies. Furthermore, the specific strategy sought to enhance Treg cells will likely vary based on the underlying defect. For example, strategies that focus on the expansion of polyclonal Treg cells may be favored over strategies that promote the generation of pTreg or iTreg cells in conditions where a defect in iTreg cell production exists. While secondary lymphoid and blood Treg cell numbers and function were largely normal or even increased in STAT3 GOF mice, we observed a defect in the in vitro and in vivo generation of iTreg and pTreg cells in STAT3 GOF mice. In patients with STAT3 GOF syndrome, defects in peripheral blood Treg cell numbers are variably observed (46). Perhaps, this may also account for some variability in the response to treatment. These data may also support the hypothesis that under conditions of immune homeostasis, STAT3 GOF Treg cells are functional and play an important role in limiting disease progression, but, under conditions of stress, such as infection or active inflammation, or in cases where other environmental or genetic factors exist, pTreg cell generation may not be sufficient to constrain dysregulated immune responses. This may, in part, contribute to the deficiency in peripheral blood Treg numbers seen

in STAT3 GOF patients. Indeed, attempts to dissect the human Treg population based on cell surface markers have demonstrated the considerable heterogeneity of this compartment, which likely also fluctuates during disease states (37, 47, 48).

The STAT3 pathway is activated downstream of numerous cytokines and growth factors and it has been broadly implicated in both innate and adaptive immune pathways (49). Studies have demonstrated that germline STAT3 GOF variants lead to alterations in human monocyte and dendritic cell populations (50). Changes in relevant antigen presenting cell phenotype and chemokine expression may have an impact on local pTreg cell induction and/or localization (33, 51). Prior work has demonstrated that although Treg cell subsets utilize similar mechanisms, unique TCR repertoires (and likely, specificity) support the notion that both peripheral and thymic-derived Treg cells are important to enforce tolerance (22, 52, 53). $CD4^+$ T cells poised to adopt a pTreg cell fate also help divert cells away from other T helper states present in the local niche, and this is best modeled by the Treg/Th17 paradigm (54). Interestingly, in the murine colitis model, we demonstrate that an increased frequency of STAT3 GOF Treg cells that had downregulated Foxp3 expression and became IL-17A-producing ex-Treg cells. In summary, these data suggest that Treg cells are less likely to be a useful primary therapeutic target for STAT3 GOF syndrome.

In our murine model on the C57BL/6 background, we did not observe spontaneous endocrinopathy, cytopenias, or other organ-specific autoimmunity such as enteropathy. It is likely that other genetic modifiers and/or environmental exposures contribute to the variability of the phenotypes that are observed in STAT3 GOF syndrome, both in mice and humans.

Surprisingly, despite the important role of STAT3 in Th17 cell generation, we did not find Th17-skewing in vivo. Rather, we observed increased IFN-γ production and Th1-skewing in the dysregulated T cells, a phenotype not typically reported to be associated with STAT3 activity. A prior study demonstrated that ex vivo stimulation of T cells from a patient with the STAT3 p.K392R variant led to increased IFN-γ and TNF-α production (20), however there is very little known about T helper cell polarization and function in STAT3 GOF. STAT3 forms homodimers, but also heterodimers with STAT1 (55). For example, STAT1 serves an important role in shaping the unique IL-27 cytokine signature (55), a cytokine that promotes early Th1 cell commitment (56, 57). It is possible that variants in STAT3 may confer alterations in STAT3 homo/heterodimer formation and DNA binding specificities, which can impact downstream transcriptomic profiles. Polarization of cells to a Th1-predominant phenotype may have implications for therapy in these patients, and would support a broader cytokine-directed approach with jakinibs or even consideration of drugs targeting type I cytokines/signaling, over a cytokine-specific therapy, such as anti-IL-6 therapy (58). Naïve T cells from STAT3 GOF mice did not demonstrate increased Th1 polarization in vitro, which suggest this is an in vivo phenomenon. Whether this is an antigen driven or independent process requires further investigation. Memory phenotype $CD4^+$ T cells have been described as a subset of cells with high expression of CD44 that are highly proliferative in the steady state and can develop in the absence of foreign antigen recognition (59). These cells have been shown to adopt an innate Th1-type effector phenotype (60). Here, we demonstrated an increased frequency of $CD4^+CD44^{hi}$ Ki-$67^+$ T cells in the STAT3 GOF mice. It will be important to explore this further, including investigation of these memory phenotype T cells in humans and autoimmune disease (61).

STAT3 also has an important role in T follicular helper (Tfh) and T follicular regulatory cell biology, and this may contribute to the apparent immune dysregulation (62). Some monogenic IEIs result in changes in the number and phenotype of circulating Tfh cells (63). An increased frequency of circulating Tfh1 cells has been observed in the peripheral blood of STAT3 GOF patients; this is a subset of Tfh cells that express defining features of Th1 cells and produce IFN-γ (64). The role of circulating Tfh1 cells in STAT3 GOF is still under investigation. It is possible that an exuberant and dysregulated circulating Tfh1 population may be contributing to autoimmunity in these cases, by enhancing the development of T-bet$^+$ B cells and humoral B cell responses that dominate in an IFN-γ governed environment, leading to a skewed Th1-type response (65). Additional studies are needed to clarify the role of these cell types in the establishment of immune dysregulation. Overall, our studies support a dysregulated T effector phenotype as a key driver of disease, rather than a primary imbalance or ineffectiveness of the Treg cell response. These results also highlight the importance of preclinical models to investigate disease mechanisms to help guide therapeutic approaches in rare diseases.

## Materials and Methods

*Generation of STAT3 GOF mice*

*Stat3*$^{p.G421R/+}$ (referred to as G421R or STAT3 GOF) mice were generated by the Hope Center Transgenic Vectors Core at Washington University School of Medicine using CRISPR-Cas9 technology (66). Please see supplemental methods for additional details. Mice were backcrossed to C57/BL6 using a speed congenic approach to ensure that they were fully backcrossed.

*Mice*

*Foxp3*$^{EGFP}$ mice were obtained from Jackson Laboratories (stock 006772) and screened per protocol listed on the Jackson Laboratories website (22). *Foxp3*$^{EGFP}$ mice were crossed to STAT3 GOF mice and NCI B6-Ly5.1/Cr congenic mice (from Charles River). *Rag1*$^{-/-}$ mice were obtained from Jackson Laboratories (stock 034159). Mice were used between 3 and 30 weeks of age, as indicated in the figures. For most studies, unless indicated, male and female mice were used between 7-16 weeks of age.

*Cell purification and adoptive transfer*

Splenocytes with or without pooled peripheral lymph nodes (axillary, brachial, inguinal) were isolated and $CD4^+$ T cells were purified with the MojoSort mouse CD4 T cell isolation kit (Cat#480005), then stained with anti-CD4 plus anti-CD45RB anti-murine antibodies, and sorted on the basis of antibody and EGFP fluorescence. Sorting was done on a BD FACS AriaFusion flow cytometer (BD Biosciences). Colitis was induced in 6-8 week old *Rag1*$^{-/-}$ mice by intraperitoneal injection of $4x10^5$ $CD4^+$ $Ly5.1^+$ $EGFP^-$ $CD45RB^{hi}$ cells isolated from WT or STAT3 GOF mice. In some experiments, mice were treated 21 days after the induction of colitis

with 1x10$^6$ CD4$^+$ Ly5.2$^+$ EGFP$^+$ WT or STAT3 GOF Treg cells. Mice were weighed at least twice weekly, and sacrificed when moribund or at the conclusion of the experiment. Mechanistic details for the lamina propria digest and isolation of lymphocytes are provided in the supplemental methods.

*Bone marrow chimeras*

Bone marrow chimeras were generated by transplanting whole bone marrow cells from Ly5.2$^+$ donors into Ly5.1$^+$ recipients that were irradiated with 2 doses of 550 cGy. 2x10$^6$ cells were injected retro-orbitally into lethally irradiated recipients. Recipients received 0.5 mg/mL sulfamethoxazole and 0.1 mg/mL trimethoprim in drinking water *ad libitum* for 2 weeks post-transplant. Cells were allowed to engraft in recipients for 12 weeks before analysis.

*Treg in vitro conversion*

Sorted CD4$^+$EGFP$^-$CD45RB$^{hi}$ naïve T cells from *Foxp3*$^{EGFP}$ and *Stat3*$^{p.G421R/+}$ *Foxp3*$^{EGFP}$ mice (1x10$^6$/ml) were cultured in R10 media (RPMI 1640 supplemented with 10% FBS, 1% penicillin-streptomycin, 1% L-glutmine), with anti-CD3 mAb (clone 145-2C11 at 10 μg/mL,BioCell Cat#BE0001-1) coated dishes in the presence of soluble anti-CD28 mAb (2 μg/mL; clone 37.51, BioCell Cat#BE0015-1), TGF-β1 (5 ng/mL; Cell Signaling Cat#5231), and 20 ng/mL IL-2 (PeproTech, Cat#212-12). In some experiments, the amount of anti-CD3 and anti-CD28 were titrated (as indicated, anti-CD3 5 μg/mL and 2.5 μg/mL, and anti-CD28 1 μg/mL). After 72h, cells were analyzed by flow cytometry.

642 *Cell stimulation for phospho-STAT3 analysis*

643 Splenic lymphocytes were isolated and cultured at $1x10^6$ cells/mL in R10 media, with or without
644 10 ng/mL recombinant murine IL-6 (Peprotech) for 15 minutes at 37ºC with 5% $CO_2$. Cells were
645 then washed with R10 and returned to 37ºC for the remaining incubation time (90 min).

646

647 *Antibodies and flow cytometry*

648 Cells were collected from the thymus, spleen, MLN, peripheral lymph nodes, colon and small
649 intestine and stained as indicated. The anti-mouse antibodies are detailed in Supplemental Table
650 2. Cells were washed with staining buffer (1X PBS containing 2% FBS and 1 mM EDTA),
651 treated with Fc block, stained with surface antibodies for 30 min at 4°C, and then washed with
652 staining buffer. Intracellular cytokine staining was performed after a 4 hour restimulation with
653 PMA (5ng/ml; Sigma-Aldrich, P1585) and ionomycin (0.5uM; Sigma-Aldrich, I0634-1MG) in
654 the presence of brefeldin A (1ul/ml; BD Biosciences). Details on phospho-flow cytometry and
655 intracellular staining are in the supplemental methods. Data was acquired on an LSRFortessa
656 (BD), or Cytek Aurora. Data was analyzed using FlowJo 10.7.1.

657

658 *Regulatory T cell suppression assay*

659 Splenocytes from *Rag1*$^{-/-}$ mice were isolated, plated, and incubated with variable numbers of
660 sorted WT and STAT3 GOF Treg cells ($CD4^+EGFP^+$) cells and TagIt violet labeled WT
661 $CD4^+EGFP^-CD45RB^{hi}$ naïve T cells in the presence of anti-CD3 (1 μg/mL). Cells were
662 incubated at 37ºC for 72h and proliferation was assessed by flow cytometry. See supplemental
663 methods for additional details.

664

*Bulk RNA sequencing*

Cell sorting for Treg cells was performed as described above. Tregs from the spleen and lymph nodes of WT or STAT3 GOF mice were pooled (3-5 mice per sample) and 4 samples for each genotype were sequenced. RNA was extracted using the RNeasy Mini Kit (Qiagen, Cat# 74014). Bulk RNA-sequencing was performed by the Genome Technology Access Center at the McDonnell Genome Institute at Washington University School of Medicine using a polyA-based amplification approach with the Takara-Clontech SMARTer low input RNA kit. See supplemental methods for details on processing and sequencing analysis.

*Bisulfite conversion and methylation analysis*

For methylation analysis, cells from male mice were used due to random X-inactivation of the *Foxp3* gene in female mice. Genomic DNA was isolated from FACS-sorted WT and STAT3 GOF EGFP$^{+}$ Treg and WT CD4$^{+}$EGFP$^{-}$CD45RB$^{hi}$ naïve T cells, according to the manufacturer's directions (Quick-DNA MiniPrep or MicroPrep, Cat#D3024 or D3020). Amplicon bisulfite sequencing was performed similar as in McDonald et al (67). Additional details on the primers, DNA libraries, sequencing, and analysis are provided in the supplemental methods.

*Single cell RNA-sequencing*

Blood samples were obtained from 6 individuals, 3 patients with STAT3 GOF syndrome and 3 age-matched healthy controls. Peripheral blood mononuclear cells (PBMCs) were isolated using Ficoll-Paque Plus (Cytiva, Cat#17-1440-02) density gradient centrifugation, subjected to RBC lysis, and frozen at -80°C before transferring for storage in liquid nitrogen. On the day of the experiment, PBMCs were thawed at 37°C, incubated in DNase I solution, filtered and then

isolated using the EasySep Human T cell Isolation Kit (Stemcell, Cat 17951) following the manufacturer's instructions. Cells were seeded at $1x10^6$ cells/ml in R10 media, and placed in a 37°C incubator with or without stimulation. Cell stimulation was performed with 25 µl/mL Immunocult Human CD3/CD28 activator reagent (Stemcell, Cat #10971) for 16 hours. Cells were filtered, washed with PBS/2% FBS/1mM EDTA, and resuspended in PBS/0.04% BSA solution for analysis. Samples were further processed by the Genome Technology Access Center at the McDonnell Genome Institute at Washington University School of Medicine where single-cell suspensions were loaded onto a Chromium Single Cell Chip (10x Genomics) according to the manufacturer's instructions.

*Single cell RNA-sequencing data processing*

Single-cell raw data was filtered, aligned and aggregated using Cellranger v6.0.0 (count and aggr functions) (68). The feature-barcode matrix analysis was performed using the R package Seurat v4 (34). In total, 147,052 cells were present in the assay. Cells with more than 15% mithochondrial RNA and less than 200 expressed features were removed, along with cells with more than 4000 features (unstimulated cells) or 6000 features (stimulated cells), and 140,931 cells remained after filtering. Data matrices were split into lists based on affected status and normalized using SCTransform. Samples were integrated based on the expression of 3000 features, and the integration anchors were identified using reciprocal PCA (RPCA) reduction with k.anchor = 20 and 30 dimensions (69). Cell types were predicted using Azimuth's human PBMC data (celltype.l2 gene list) (69). Cells classified as anything other than T cells subsets were filtered out, and with that, 139,421 cells remained. For differential expression between STAT3 GOF and control samples, the data was log normalized (scale = 10000) and the Seurat's

711 “FindVariableFeatures” function with default parameters was used, and to calculate average
712 expression. Heatmaps of statistically significant differentially expressed genes (adjusted p-value
713 <0.05, Log2FC >0.25 or <-0.25) were generated using bulk average RNA expression of
714 normalized counts with the AverageExpression() function in R for each condition. Differential
715 expression gene lists were generated based on the non-parametric Wilcoxon rank sum test.
716 Pathway analysis was performed using Metascape (70). Only genes with adjusted p-value < 0.05
717 were retained for pathway analysis. Figures were generated using Seurat, dittoseq and
718 EnhancedVolcano R packages (https://github.com/kevinblighe/EnhancedVolcano) (34, 69). Data
719 has been deposited under accession number GSE207936.
720
721 *Statistics*
722 Statistical details of experiments can be found in figure legends including number of
723 experimental replicates and/or number of animals and the number of independent times an
724 experiment was performed. Statistics were calculated using Prism 9 and the specific test is
725 designated in the figure legends. In general, an unpaired t test was used for all comparisons with
726 two groups and Welch’s t test was used in the instance of unequal variance. For comparisons
727 with 3 or more groups samples were analyzed with a one-way ANOVA (with Turkey’s multiple
728 comparisons test) or a Welch ANOVA if the variance was unequal (with Dunnett’s multiple
729 comparisons test). In instances with two variables, a two-way ANOVA was performed. The
730 comparisons between groups for overall survival functions were done using the log-rank test. We
731 contrasted weight change profiles between groups using a random coefficient model with
732 quadratic day terms and group interaction with the quadratic day terms (SAS 9.4 mixed

procedure) (71). Degrees of freedom were adjusted with the Kenward-Roger method for bias correction.

*Study approval*

Animal studies were approved by the IACUC at Washington University. Human blood samples were sourced ethically and research use was in accord with the terms of the informed consent under IRB approved protocols at the author's institutions.

**Author contributions**

E.G.S. and M.A.C. designed the work and wrote the manuscript; E.G.S, K.A.T., S.R., N.S., Z.J.G. and R.F. performed experiments. E.G.S., K.A.T., A.K., J.R.E., and M.A.C. analyzed and interpreted the data; T.PV. designed and performed experiments. J.W.L., J.J.B., and A.T. provided patient samples and contributed to the manuscript. L.G.S. supervised experiments.

**Acknowledgements**

We would like to thank Kelsey Trammel and Molly Keppel for technical assistance. We thank the Genome Technology Access Center at the McDonnell Genome Institute at Washington University School of Medicine for help with genomic analysis. The Center is partially supported by NCI Cancer Center Support Grant #P30 CA91842 to the Siteman Cancer Center from the National Center for Research Resources (NCRR), a component of the National Institutes of Health (NIH), and NIH Roadmap for Medical Research. This publication is solely the responsibility of the authors and does not necessarily represent the official view of NCRR or NIH. This work was supported by the Hope Center Transgenic Vectors Core at Washington

University School of Medicine. Michael Wallendorf provided Biostatistical support for the murine colitis studies.

**Grant Support**

E.G.S. was supported by NIH grants K12HD076224, T32 HD 43010, and T32 AI 106688, and a Rheumatic Diseases Research Resource-based Center (RDRRC) at Washington University Pilot and Feasibility Grant (NIH P30AR073752). Grant support was received from NIH/NIAID 1P01AI155393, the National Scleroderma Foundation, the Crohn's and Colitis Foundation, the Washington University Digestive Disease Research Core Center (NIH 5P30DK052574), the RDRRC NIH P30AR48335, and the Children's Discovery Institute at St. Louis Children's Hospital and Washington University (to M.A.C.).

**Abbreviations**

APECED, autoimmune polyendocrinopathy with candidiasis and ectodermal dystrophy; CNS2, conserved noncoding sequencing 2; GOF, gain-of-function; HOM, homozygous; IEI, inborn errors of immunity; IPEX, immune dysregulation, polyendocrinopathy, enteropathy, X-linked syndrome; LN, lymph node; MLN, mesenteric lymph node; PIRD, primary immune regulatory disorders; Tfh, T follicular helper cell; TSDR, Treg-specific demethylation region

## References


1. Bousfiha A, et al. Human Inborn Errors of Immunity: 2019 Update of the IUIS Phenotypical Classification. *J Clin Immunol.* 2020;40(1):66-81.
2. Tangye SG, et al. Human Inborn Errors of Immunity: 2019 Update on the Classification from the International Union of Immunological Societies Expert Committee. *Journal of Clinical Immunology.* 2020;40(1):24-64.
3. Chan AY, and Torgerson TR. Primary immune regulatory disorders: a growing universe of immune dysregulation. *Current Opinion in Allergy and Clinical Immunology.* 2020;20(6):582-90.
4. Powell BR, et al. An X-linked syndrome of diarrhea, polyendocrinopathy, and fatal infection in infancy. *J Pediatr.* 1982;100(5):731-7.
5. Chatila TA, et al. JM2, encoding a fork head-related protein, is mutated in X-linked autoimmunity-allergic disregulation syndrome. *J Clin Invest.* 2000;106(12):R75-81.
6. Bennett CL, et al. The immune dysregulation, polyendocrinopathy, enteropathy, X-linked syndrome (IPEX) is caused by mutations of FOXP3. *Nature Genetics.* 2001;27(1):20-1.
7. Wildin RS, et al. X-linked neonatal diabetes mellitus, enteropathy and endocrinopathy syndrome is the human equivalent of mouse scurfy. *Nature Genetics.* 2001;27(1):18-20.
8. Chatila TA, et al. JM2, encoding a fork head–related protein, is mutated in X-linked autoimmunity–allergic disregulation syndrome. *The Journal of Clinical Investigation.* 2000;106(12):R75-R81.
9. Cepika AM, et al. Tregopathies: Monogenic diseases resulting in regulatory T-cell deficiency. *J Allergy Clin Immunol.* 2018;142(6):1679-95.
10. Aaltonen J, et al. An autoimmune disease, APECED, caused by mutations in a novel gene featuring two PHD-type zinc-finger domains. *Nature Genetics.* 1997;17(4):399-403.
11. Nagamine K, et al. Positional cloning of the APECED gene. *Nature Genetics.* 1997;17(4):393-8.
12. Anderson MS, et al. Projection of an Immunological Self Shadow Within the Thymus by the Aire Protein. *Science.* 2002;298(5597):1395-401.
13. Milner JD, et al. Early-onset lymphoproliferation and autoimmunity caused by germline STAT3 gain-of-function mutations. *Blood.* 2015;125(4):591-9.
14. Fabre A, et al. Clinical Aspects of STAT3 Gain-of-Function Germline Mutations: A Systematic Review. *J Allergy Clin Immunol Pract.* 2019;7(6):1958-69.e9.
15. Villarino AV, et al. Mechanisms and consequences of Jak–STAT signaling in the immune system. *Nature Immunology.* 2017;18(4):374-84.
16. Wei L, et al. New insights into the roles of Stat5a/b and Stat3 in T cell development and differentiation. *Semin Cell Dev Biol.* 2008;19(4):394-400.
17. Khoury T, et al. Tocilizumab Promotes Regulatory T-cell Alleviation in STAT3 Gain-of-function-associated Multi-organ Autoimmune Syndrome. *Clin Ther.* 2017;39(2):444-9.
18. Lin L, et al. The clinical, immunological and genetic features of 12 Chinese patients with STAT3 mutations. *Allergy Asthma Clin Immunol.* 2020;16:65.
19. Wang W, et al. Efficacy of tocilizumab therapy in a patient with severe pancytopenia associated with a STAT3 gain-of-function mutation. *BMC Immunol.* 2021;22(1):19.
20. Flanagan SE, et al. Activating germline mutations in STAT3 cause early-onset multi-organ autoimmune disease. *Nat Genet.* 2014;46(8):812-4.

21. Haapaniemi EM, et al. Autoimmunity, hypogammaglobulinemia, lymphoproliferation, and mycobacterial disease in patients with activating mutations in STAT3. *Blood.* 2015;125(4):639-48.
22. Haribhai D, et al. Regulatory T Cells Dynamically Control the Primary Immune Response to Foreign Antigen. *The Journal of Immunology.* 2007;178(5):2961-72.
23. Floess S, et al. Epigenetic Control of the foxp3 Locus in Regulatory T Cells. *PLOS Biology.* 2007;5(2):e38.
24. Huehn J, and Beyer M. Epigenetic and transcriptional control of Foxp3+ regulatory T cells. *Seminars in Immunology.* 2015;27(1):10-8.
25. Feng Y, et al. Control of the Inheritance of Regulatory T Cell Identity by a cis Element in the Foxp3 Locus. *Cell.* 2014;158(4):749-63.
26. Toker A, et al. Active demethylation of the Foxp3 locus leads to the generation of stable regulatory T cells within the thymus. *J Immunol.* 2013;190(7):3180-8.
27. Hill JA, et al. Foxp3 Transcription-Factor-Dependent and -Independent Regulation of the Regulatory T Cell Transcriptional Signature. *Immunity.* 2007;27(5):786-800.
28. Zheng Y, et al. Genome-wide analysis of Foxp3 target genes in developing and mature regulatory T cells. *Nature.* 2007;445(7130):936-40.
29. Rudra D, et al. Transcription factor Foxp3 and its protein partners form a complex regulatory network. *Nature Immunology.* 2012;13(10):1010-9.
30. Chaudhry A, et al. CD4+ regulatory T cells control TH17 responses in a Stat3-dependent manner. *Science.* 2009;326(5955):986-91.
31. Powrie F, et al. Phenotypically distinct subsets of CD4+ T cells induce or protect from chronic intestinal inflammation in C. B-17 scid mice. *Int Immunol.* 1993;5(11):1461-71.
32. Izcue A, et al. Regulatory T cells suppress systemic and mucosal immune activation to control intestinal inflammation. *Immunol Rev.* 2006;212:256-71.
33. Haribhai D, et al. Alternatively Activated Macrophages Boost Induced Regulatory T and Th17 Cell Responses during Immunotherapy for Colitis. *J Immunol.* 2016;196(8):3305-17.
34. Hao Y, et al. Integrated analysis of multimodal single-cell data. *Cell.* 2021;184(13):3573-87 e29.
35. Ferraro A, et al. Interindividual variation in human T regulatory cells. *Proc Natl Acad Sci U S A.* 2014;111(12):E1111-20.
36. Göschl L, et al. Treg cells in autoimmunity: from identification to Treg-based therapies. *Seminars in Immunopathology.* 2019;41(3):301-14.
37. Sakaguchi S, et al. Regulatory T Cells and Human Disease. *Annu Rev Immunol.* 2020;38:541-66.
38. Schmitt EG, et al. Chronic follicular bronchiolitis requires antigen-specific regulatory T cell control to prevent fatal disease progression. *J Immunol.* 2013;191(11):5460-76.
39. Levescot A, et al. IL-1β-driven osteoclastogenic Tregs accelerate bone erosion in arthritis. *The Journal of clinical investigation.* 2021;131(18):e141008.
40. Warshauer JT, et al. A human mutation in STAT3 promotes type 1 diabetes through a defect in CD8+ T cell tolerance. *J Exp Med.* 2021;218(8).
41. Brunkow ME, et al. Disruption of a new forkhead/winged-helix protein, scurfin, results in the fatal lymphoproliferative disorder of the scurfy mouse. *Nature Genetics.* 2001;27(1):68-73.

42. Steward-Tharp SM, et al. A mouse model of HIES reveals pro- and anti-inflammatory functions of STAT3. *Blood.* 2014;123(19):2978-87.
43. Boardman DA, and Levings MK. Emerging strategies for treating autoimmune disorders with genetically modified Treg cells. *J Allergy Clin Immunol.* 2022;149(1):1-11.
44. Mikami N, et al. New Treg cell-based therapies of autoimmune diseases: towards antigen-specific immune suppression. *Current Opinion in Immunology.* 2020;67:36-41.
45. Sato Y, et al. Human-engineered Treg-like cells suppress FOXP3-deficient T cells but preserve adaptive immune responses in vivo. *Clin Transl Immunology.* 2020;9(11):e1214.
46. Jagle S, et al. Distinct molecular response patterns of activating STAT3 mutations associate with penetrance of lymphoproliferation and autoimmunity. *Clin Immunol.* 2020;210:108316.
47. Lam AJ, et al. Helios is a marker, not a driver, of human Treg stability. *Eur J Immunol.* 2022;52(1):75-84.
48. Opstelten R, et al. GPA33: A Marker to Identify Stable Human Regulatory T Cells. *J Immunol.* 2020;204(12):3139-48.
49. Hillmer EJ, et al. STAT3 signaling in immunity. *Cytokine & Growth Factor Reviews.* 2016;31:1-15.
50. Korenfeld D, et al. STAT3 Gain-of-Function Mutations Underlie Deficiency in Human Nonclassical CD16+ Monocytes and CD141+ Dendritic Cells. *The Journal of Immunology.* 2021;207(10):2423-32.
51. Russler-Germain EV, et al. Gut Helicobacter presentation by multiple dendritic cell subsets enables context-specific regulatory T cell generation. *Elife.* 2021;10:e54792.
52. Lathrop SK, et al. Peripheral education of the immune system by colonic commensal microbiota. *Nature.* 2011;478(7368):250-4.
53. Relland LM, et al. The TCR repertoires of regulatory and conventional T cells specific for the same foreign antigen are distinct. *J Immunol.* 2012;189(7):3566-74.
54. Bettelli E, et al. Reciprocal developmental pathways for the generation of pathogenic effector TH17 and regulatory T cells. *Nature.* 2006;441(7090):235-8.
55. Hirahara K, et al. Asymmetric Action of STAT Transcription Factors Drives Transcriptional Outputs and Cytokine Specificity. *Immunity.* 2015;42(5):877-89.
56. Lucas S, et al. IL-27 regulates IL-12 responsiveness of naive CD4+ T cells through Stat1-dependent and -independent mechanisms. *Proceedings of the National Academy of Sciences.* 2003;100(25):15047-52.
57. Takeda A, et al. Cutting Edge: Role of IL-27/WSX-1 Signaling for Induction of T-Bet Through Activation of STAT1 During Initial Th1 Commitment. *The Journal of Immunology.* 2003;170(10):4886-90.
58. Forbes LR, et al. Jakinibs for the treatment of immune dysregulation in patients with gain-of-function signal transducer and activator of transcription 1 (STAT1) or STAT3 mutations. *J Allergy Clin Immunol.* 2018;142(5):1665-9.
59. Younes SA, et al. Memory phenotype CD4 T cells undergoing rapid, nonburst-like, cytokine-driven proliferation can be distinguished from antigen-experienced memory cells. *PLoS Biol.* 2011;9(10):e1001171.
60. Kawabe T, et al. Memory-phenotype CD4(+) T cells spontaneously generated under steady-state conditions exert innate TH1-like effector function. *Sci Immunol.* 2017;2(12).

61. Kawabe T, and Sher A. Memory-phenotype CD4+ T cells: a naturally arising T lymphocyte population possessing innate immune function. *Int Immunol.* 2022;34(4):189-96.
62. Hart AP, and Laufer TM. A review of signaling and transcriptional control in T follicular helper cell differentiation. *Journal of Leukocyte Biology.* 2022;111(1):173-95.
63. Ma CS, et al. Monogenic mutations differentially affect the quantity and quality of T follicular helper cells in patients with human primary immunodeficiencies. *Journal of Allergy and Clinical Immunology.* 2015;136(4):993-1006.e1.
64. Tangye SG, and Ma CS. Molecular regulation and dysregulation of T follicular helper cells – learning from inborn errors of immunity. *Current Opinion in Immunology.* 2021;72:249-61.
65. Knox JJ, et al. T-bet(+) memory B cells: Generation, function, and fate. *Immunological reviews.* 2019;288(1):149-60.
66. Ran FA, et al. Genome engineering using the CRISPR-Cas9 system. *Nat Protoc.* 2013;8(11):2281-308.
67. McDonald JI, et al. Reprogrammable CRISPR/Cas9-based system for inducing site-specific DNA methylation. *Biol Open.* 2016;5(6):866-74.
68. Zheng GX, et al. Massively parallel digital transcriptional profiling of single cells. *Nat Commun.* 2017;8:14049.
69. Stuart T, et al. Comprehensive Integration of Single-Cell Data. *Cell.* 2019;177(7):1888-902 e21.
70. Zhou Y, et al. Metascape provides a biologist-oriented resource for the analysis of systems-level datasets. *Nat Commun.* 2019;10(1):1523.
71. Loughin TM. SAS® for Mixed Models, 2nd edition Edited by Littell, R. C., Milliken, G. A., Stroup, W. W., Wolfinger, R. D., and Schabenberger, O. *Biometrics.* 2006;62(4):1273-4.

## Figures and legends

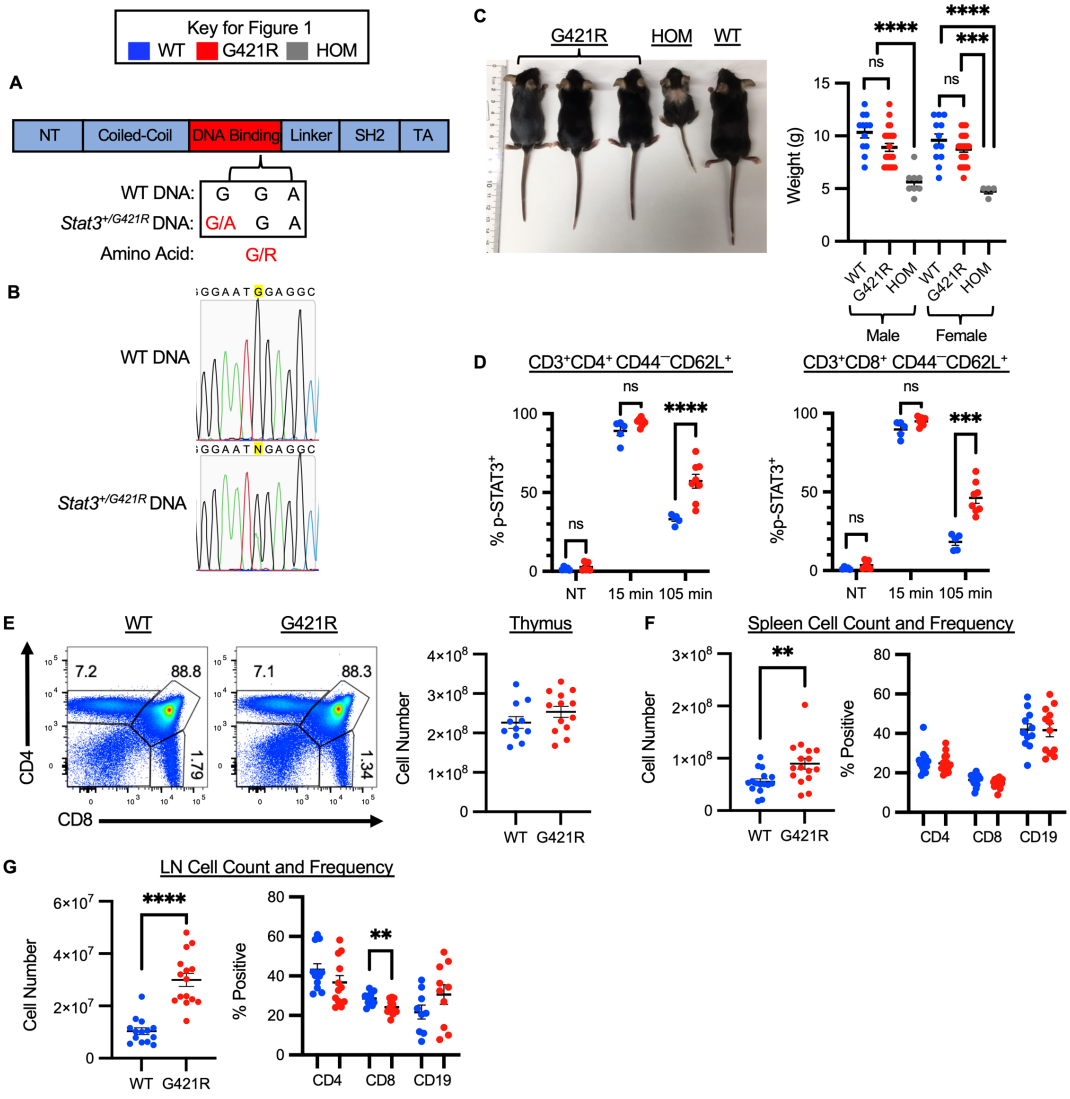


**Figure 1. Generation of the STAT3 GOF mice. (A)** STAT3 p.G421R variant located in the DNA-binding domain was inserted into WT mice using CRISPR-Cas9. NT, N-terminal; TA, transactivation domain. **(B)** The point mutation was confirmed by sanger sequencing. **(C)** WT, G421R (*Stat3*$^{p.G421R/+}$) and HOM (*Stat3*$^{p.G421R/\ p.G421R}$) littermates at 38 days of age (left) and weaning weight of male and female littermates (right). **(D)** Splenocytes from WT and G421R mice were stimulated with IL-6 for 15 min, washed and then analyzed or returned to culture for the indicated time prior to analysis for p-STAT3. **(E)** Representative flow cytometry from the thymus of 3-4 week old mice (left) and thymus cell counts (right). **(F)** Scatter plot showing adult mice spleen cell counts and frequency of $CD3^+CD4^+$, $CD3^+CD8^+$, and $CD3^-CD19^+$ cells within the live cell gate. **(G)** Scatter plot showing adult mice pooled peripheral lymph node (axillary, brachial, inguinal) cell counts and frequency of $CD3^+CD4^+$, $CD3^+CD8^+$, and $CD3^-CD19^+$ cells within the live cell gate. For all scatter plots, each dot represents an individual mouse, the lines represent the mean with error bars representing the SEM. Data are representative of at least 3 independent experiments, except for (D) which represents 2 independent experiments. For these and all subsequent figures, young mice: <6wk of age, adult mice: age 7-16wk; old mice: age

>20wk. An unpaired t test was used for all comparisons with two groups and Welch's t test was used in the instance of unequal variance, and for those with 3 or more groups a one-way ANOVA was used except for in (D) which was analyzed with a two-way ANOVA. *$p<0.05$, **$p<0.01$, ***$p<0.001$, ****$p<0.0001$.

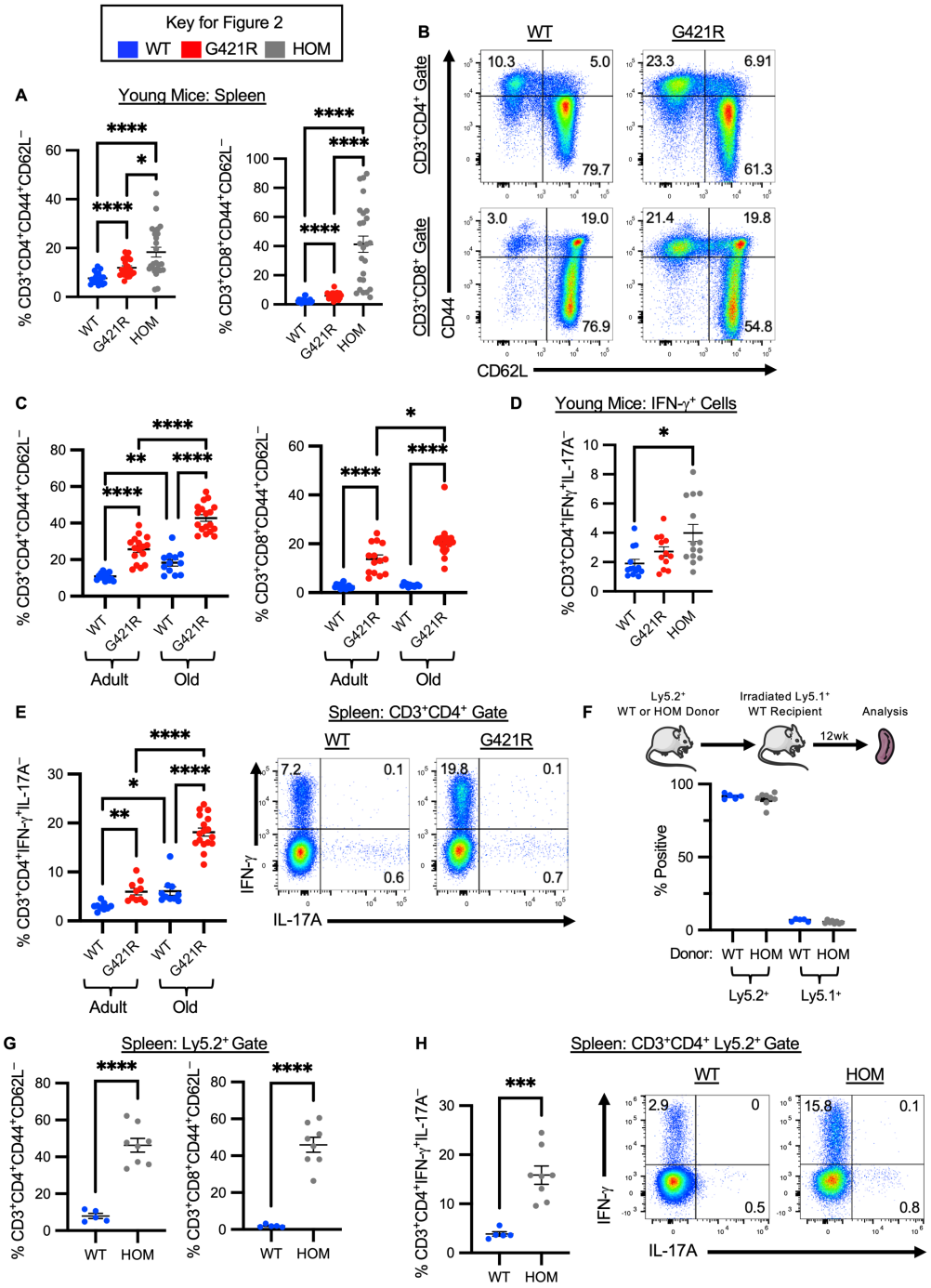


**Figure 2. T cell dysregulation in STAT3 GOF mice. (A)** Frequency of $CD3^+CD4^+CD44^+CD62L^-$ or $CD3^+CD8^+CD44^+CD62L^-$ T cells in the spleen of young mice. **(B)** Representative flow cytometry from the spleen of adult mice. **(C)** Frequency of $CD3^+CD4^+CD44^+CD62L^-$ or $CD3^+CD8^+CD44^+CD62L^-$ T cells in the spleen of adult and old mice. **(D)** Frequency of $CD3^+CD4^+IFN\text{-}\gamma^+IL\text{-}17A^-$ cells in the spleen of young mice. **(E)** Scatter plot showing adult and old mice spleen frequency of $CD3^+CD4^+IFN\text{-}\gamma^+IL\text{-}17A^-$ cells (left) and representative flow cytometry from the spleen of old mice (right). **(F)** Graphical representation of experimental outline for BM transplant (top). Frequency of $Ly5.2^+$ or $Ly5.1^+$ cells in the

spleen of transplanted mice, gated on live, single cells. Data are representative of 3-4 independent experiments, n=8 HOM→WT, and n=5 WT→WT. **(G)** Frequency of donor Ly5.2$^+$ cells that were CD3$^+$CD4$^+$CD44$^+$CD62L$^-$ or CD3$^+$CD8$^+$CD44$^+$CD62L$^-$ in the spleen of transplanted mice. **(H)** Percentage of donor Ly5.2$^+$ cells that were CD3$^+$CD4$^+$IFN-$\gamma^+$IL-17A$^-$ (left) and representative flow cytometry from the spleen of transplanted mice (right). For all scatter plots, each dot represents an individual mouse, the lines represent the mean with error bars representing the SEM. Data are representative of at least 3 independent experiments. An unpaired t test was used for all comparisons with two groups and Welch's t test was used in the instance of unequal variance, and for those with 3 or more groups a one-way ANOVA. *$p<0.05$, **$p<0.01$, ***$p<0.001$, ****$p<0.0001$.

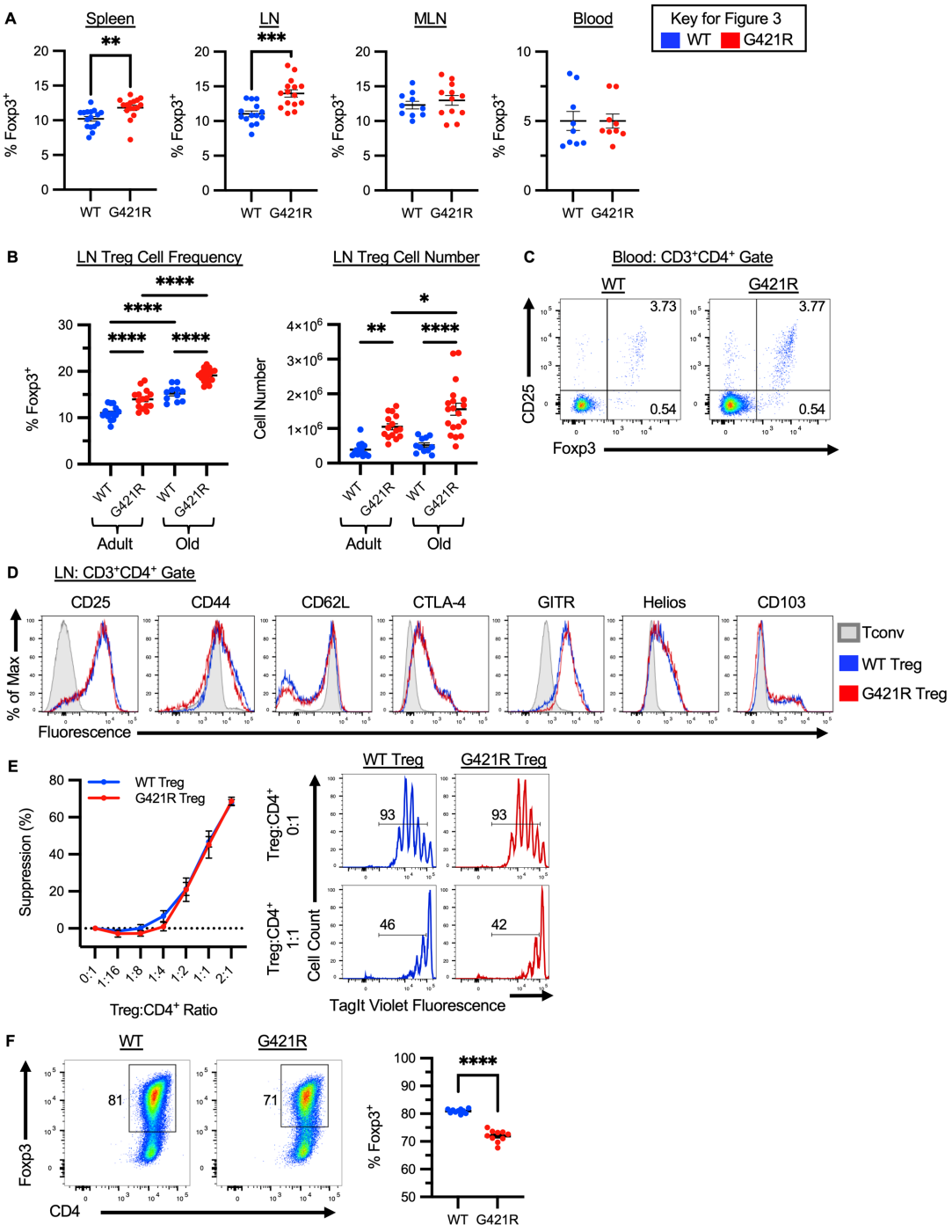


**Figure 3. Treg cells in STAT3 GOF mice. (A)** Frequency of $CD3^+CD4^+Foxp3^+$ Treg cells in the indicated tissues of adult mice. **(B)** Percentage (left) and number (right) of $CD3^+CD4^+$ $Foxp3^+$ Treg cells in the peripheral lymph node of adult and old mice. **(C)** Representative flow cytometry from the peripheral blood of adult mice. **(D)** Representative flow cytometry from the peripheral lymph node showing staining for the indicated markers, gated on WT Tconv ($CD3^+CD4^+Foxp3$-EGFP$^-$), or Treg cells ($CD3^+CD4^+Foxp3$-EGFP$^+$) from WT and G421R mice. Data are representative of at least 9 mice and 4 independent experiments. **(E)** Suppressive capacity of WT and G421R Treg cells as measured by TagIt violet dilution on responder T cells.

Graph depicting the average and SEM of the percent suppression, at each Treg to CD4 ratio (left). Representative histograms are shown along with the average proliferation of $CD4^+$ T cells for selected Treg to CD4 ratios (right). Percent suppression = (percent proliferation of the $CD4^+$ T cells at the 0:1 Treg:Teff ratio — percent proliferation of $CD4^+$ T cells for each Treg to CD4 ratio) ÷ percent proliferation of the $CD4^+$ T cells at the 0:1 Treg:Teff ratio. Data were from 3 experiments consisting of 8-9 individual assays. **(F)** In-vitro derived iTreg cells were generated from WT or G421R $CD4^+EGFP^-CD45RB^{hi}$ naïve T cells with TCR cross-linking, TGF-β1, and IL-2. Representative flow cytometry (left) and scatter plot showing the frequency of $CD4^+Foxp3^+$ Treg cells (right). Each point represents an individual mouse and at least 3 independent experiments. An unpaired t test was used for comparisons with two groups, a Welch's t test was used for unequal variance, and for 3 or more groups a one-way ANOVA was used except for in (E) which was analyzed with a two-way ANOVA. *$p<0.05$, **$p<0.01$, ***$p<0.001$, ****$p<0.0001$.

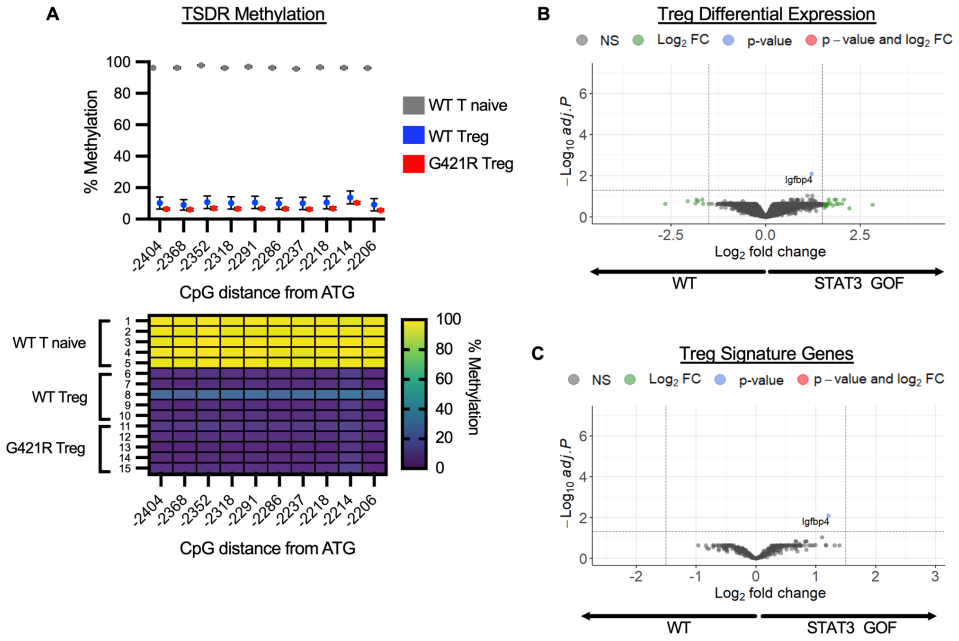


**Figure 4. Epigenetic and transcriptional profile of Treg cells. (A)** Methylation status of ten individual CpG motifs within the Treg specific demethylation region (TSDR) in the *Foxp3* locus. Individual CpG motifs are numbered in reference to the translational start site. The average percent methylation is shown in the dot plot (top) for WT T naïve cells, WT Treg and G421R Treg isolated from the spleen and peripheral LN of adult mice (n=5 for each group). Methylation patterns of each of the examined TSDR motifs of Tregs and naïve T cells are shown in the heat map (bottom). The color code ranges from purple (no methylation) to yellow (100% methylation). **(B)** Fold-change vs. P-value (volcano) plot of gene expression in purified STAT3 GOF Treg cells compared to WT Treg cells (n=4 samples for each genotype, with 3-5 pooled mice for each sample). Differential expression analysis was performed and the results were filtered for only those genes with Benjamini-Hochberg false-discovery rate adjusted p-values less than or equal to 0.05. **(C)** Fold-change vs. P-value (volcano) plot of gene expression in purified STAT3 GOF Treg cells compared to WT Treg cells of a subset of transcripts assigned to the Treg cell signature transcriptome. Transcripts with a log2 fold change >1.5 or < –1.5 and p<0.05 are considered significant.

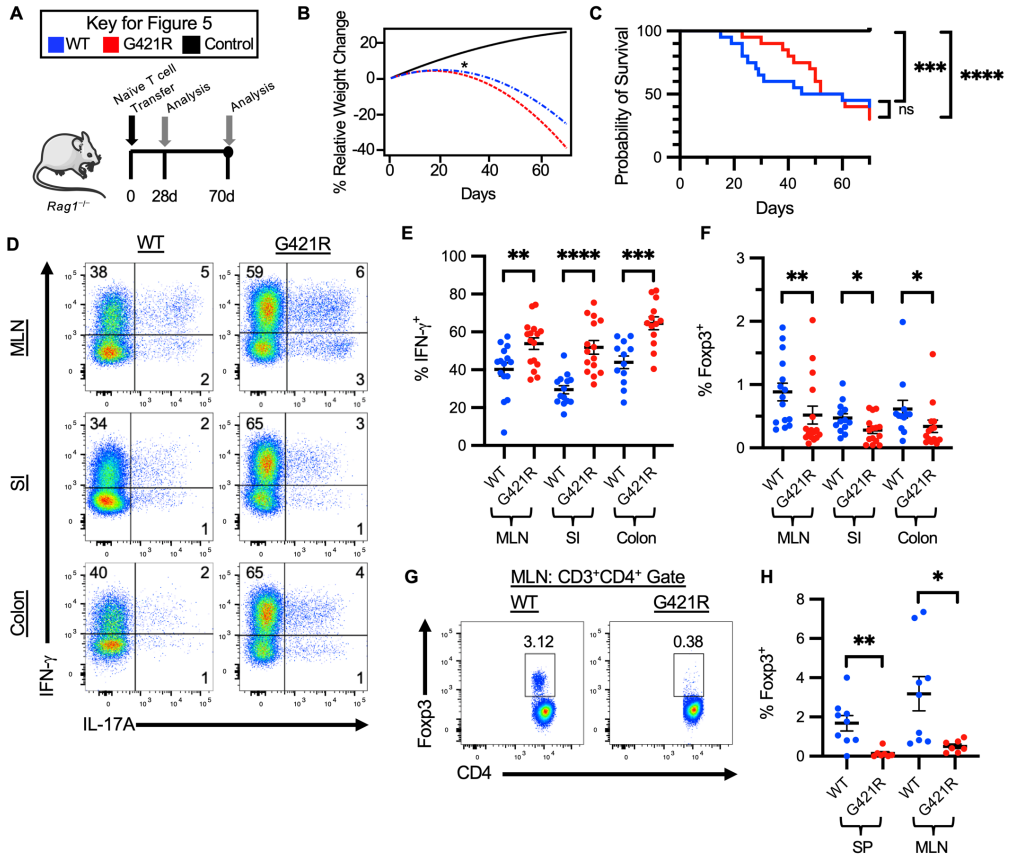


**Figure 5. Th1-skewing and reduced pTreg generation in a colitis model. (A)** Experimental design for establishment of the lymphopenia-induced colitis model. **(B)** Quadratic regression analysis modeling the percent relative weight change over time after the induction of experimental colitis with naïve T cells isolated from WT (n=20) or G421R mice (n=20) compared to control C57BL/6J *Rag1*$^{-/-}$ mice (n=14). *represents day 28, at which a significant reduction in the weight was observed in colitis mice as compared to control mice. **(C)** Kaplan-Meier survival curves for the mice in (B). Comparisons for the survival functions were done using the log-rank test. **(D)** Representative flow cytometry of $CD3^+CD4^+$ T cells isolated from the MLN, colon and SI lamina propria lymphocytes and restimulated with PMA/ionomycin. Data was obtained at 28 days after the induction of experimental colitis. **(E)** Frequency of IFN-γ-producing $CD3^+CD4^+$ T cells in the indicated tissues, 28 days after induction of experimental colitis. **(F)** Percentage of in-vivo derived pTreg cells ($CD3^+CD4^+$ $Foxp3^+$) in the indicated tissues, 28 days after the induction of experimental colitis. **(G)** Representative flow cytometry from the MLN showing pTreg cell induction in mice that survived to the conclusion of the experiment (70d). **(H)** Frequency of pTreg cells ($CD3^+CD4^+$ $Foxp3^+$) in the spleen and MLN of mice with WT or G421R colitis, that survived to day 70. An unpaired t test was used for all comparisons with two groups and Welch's t test was used in the instance of unequal variance. *p<0.05, **p<0.01, ***p<0.001, ****p<0.0001.

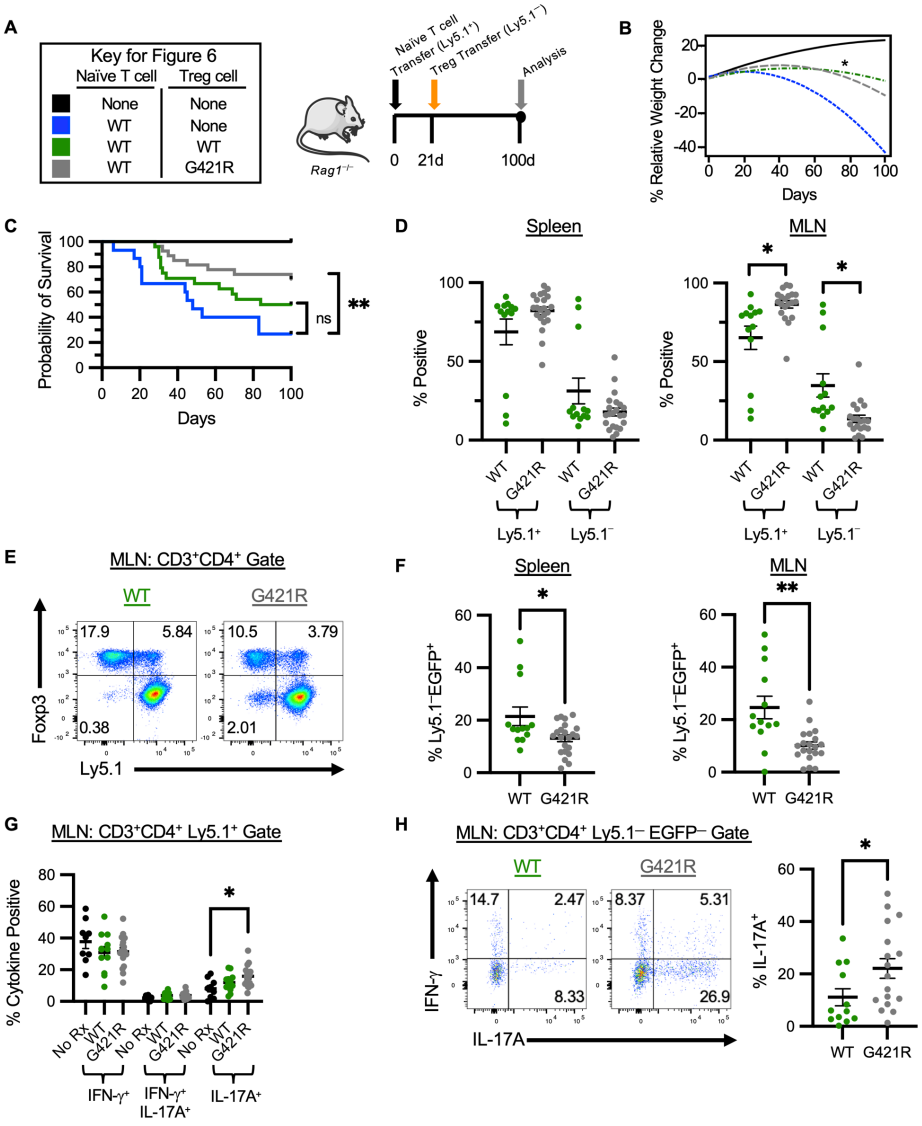


**Figure 6. STAT3 GOF Treg cells are functional in vivo. (A)** Experimental design for the Treg treatment studies using the lymphopenia-induced colitis model. **(B)** Quadratic regression analysis modeling the percent relative weight change over time after the induction of experimental colitis with naïve T cells isolated from WT mice. Mice were treated on day 21 with $1x10^6$ WT Treg cells (n=24) or G421R Treg cells (n=27) and weight patterns were compared to untreated mice (n=15) or control C57BL/6J *Rag1*$^{-/-}$ mice (n=6). *represents day 77, at which a significant increase in the weight was observed in colitis mice treated with WT Treg cells as compared to untreated mice. **(C)** Kaplan-Meier survival curves for the mice in (B). Comparisons for the survival functions were done using the log-rank test. **(D)** Percentage of colitogenic Ly5.1$^+$ T cells and Ly5.1$^-$ T cells (treatment) isolated from the spleen and MLN of treated mice. **(E)** Representative flow cytometry from the MLN of treated mice showing Treg cell recovery. **(F)** Frequency of transferred Ly5.1$^-$ WT or G421R Treg cells recovered in the spleen and MLN of treated mice. **(G)** Frequency of MLN CD3$^+$CD4$^+$Ly5.1$^+$ T cells that produce IFN-γ, both IFN-γ and IL-17A, or just IL-17A after stimulation with PMA/ionomycin. **(H)** Representative flow

cytometry from the MLN of treated mice, demonstrating ex-Treg cell ($CD3^+CD4^+Ly5.1^-$ $EGFP^-$) cytokine production after restimulation with PMA/ionomycin (left). Scatter plot demonstrating the frequency of MLN ex-Treg cells ($CD3^+CD4^+Ly5.1^-$ $EGFP^-$) that produce IL-17A (right). An unpaired t test was used for all comparisons with two groups and Welch's t test was used in the instance of unequal variance, and for those with 3 or more groups a one-way ANOVA was used. *$p<0.05$, **$p<0.01$.

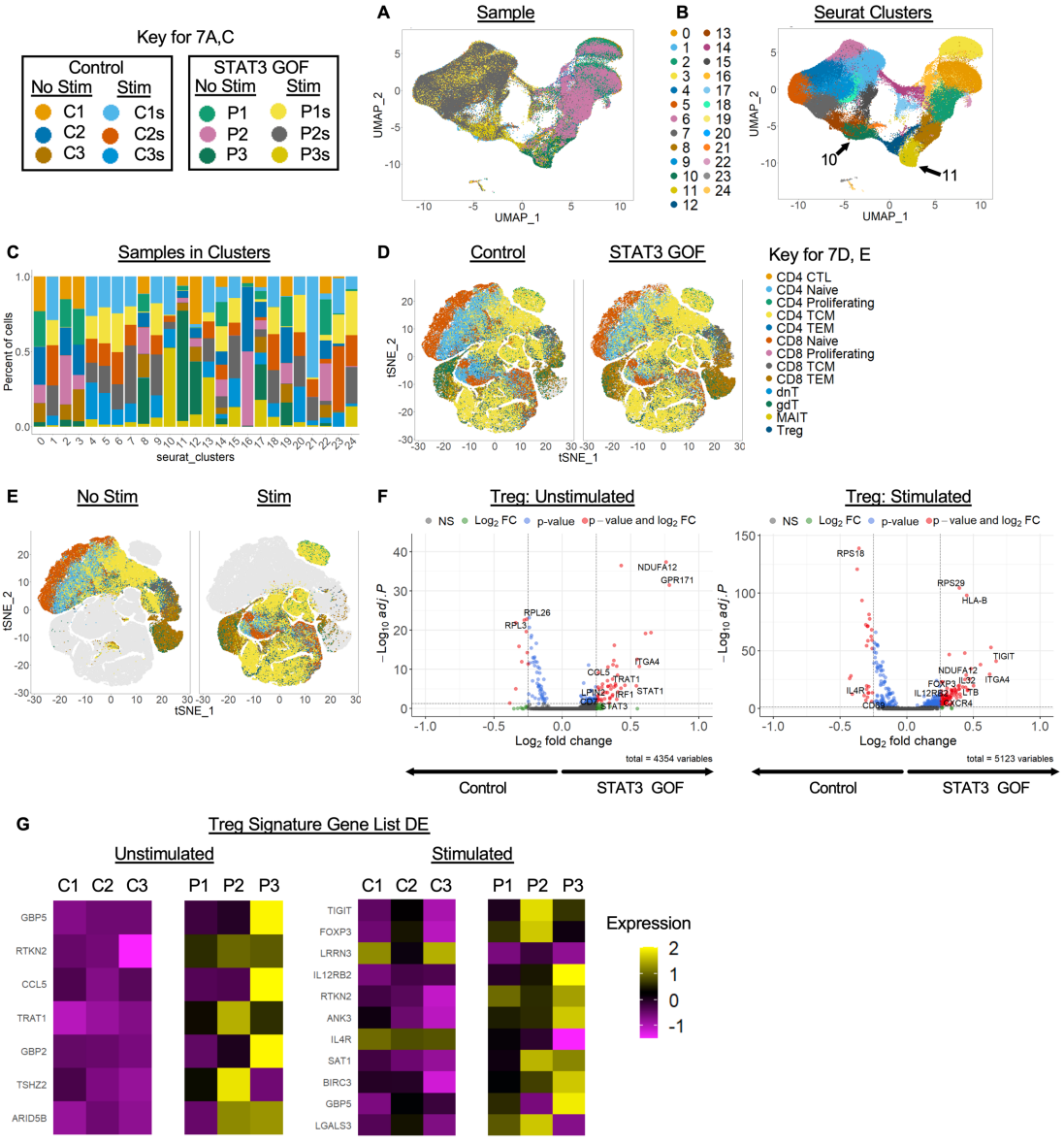


**Figure 7. STAT3 GOF syndrome T cell single cell RNA-sequencing.** Control and patient T cells were isolated from PBMCs by CD3-negative selection, then incubated in media alone (no stimulation) or with anti-CD3/CD28 stimulation for 16h before submitting for scRNA-sequencing analysis. Unsupervised dimensionality reduction analysis of single cell RNA-sequencing transcriptome data from STAT3 GOF and healthy controls showing sample identity **(A)** and unique clusters **(B)**. **(C)** Cluster composition as defined by sample identity. Identification of cells using Azimuth cell prediction program with tSNE plot showing T cells split based on the affected status **(D)** or by stimulation status **(E)**. **(F)** Volcano plot showing differential expression (adjusted p-value <0.05, average log2fc >0.25 or < –0.25) in cells identified as Tregs, comparing cells from unstimulated (top) or stimulated conditions (bottom). **(G)** Heatmap showing the average log2 fold change of differentially expressed genes found in the Treg cell signature gene list for control and STAT3 GOF Treg cells.

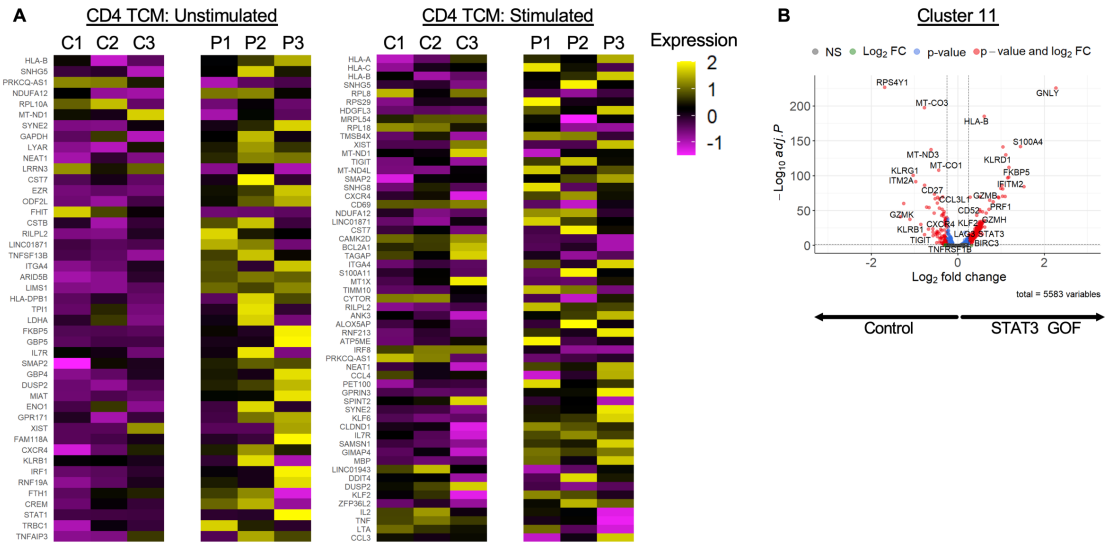


**Figure 8. Transcriptional changes in STAT3 GOF patient T cells. (A)** Heatmap showing the average log2 fold change of differentially expressed genes found in unstimulated and stimulated T central memory cells identified by the Azimuth cell prediction program in Figure 7D. **(B)** Volcano plot showing differential expression in cells from cluster 11 identified in the UMAP plot in Figure 7B.